Development of Slippery Liquid-Infused Porous Surfaces (SLIPS) using Suspension Plasma Spray

Hani Jazaerli

A Thesis
In the Department
of
Mechanical, Industrial and Aerospace Engineering

Presented in Partial Fulfillment of the Requirements
for the Degree of
Master of Applied Sciences (Mechanical Engineering) at
Concordia University
Montreal, Quebec, Canada

April 2019

CONCORDIA UNIVERSITY

School of Graduate Studies

This is to certify that the thesis prepared

By: Hani Jazaerli

Entitled: Development of Slippery Liquid-Infused Porous Surfaces (SLIPS) using Suspension Plasma Spray

And submitted in partial fulfilment of the requirements for the degree of

Master of Applied Sciences (Mechanical Engineering)

Complies with the regulations of the University and meets the accepted standards with respect to originality and quality.

Signed by the final Examining Committee:

_____ Chair
Mojtaba Kheiri

_____ External Examiner
Sana Anbuhi

_____ External to Program

_____ Examiner
Farjad Shadmehri

_____ Examiner

_____ Thesis Supervisor
Ali Dolatabadi

_____ Thesis Co-Supervisor
Christian Moreau

_____ Thesis Co-Supervisor
Martin Pugh

Approved by: _____
Chair of Department or Graduate Program Director

_____ 2019 _____ Dean of Faculty

ABSTRACT

Development of Slippery Liquid-Infused Porous Surfaces (SLIPS) using Suspension Plasma Spray

Hani Jazaerli

Ice accumulation on aerodynamic surfaces of aircrafts is one of the major threats facing aerospace companies. A potential solution to alleviate the problems caused by aircraft icing is the development of a slippery surface that can delay ice build-up and facilitate its removal. Using suspension plasma spraying of submicron-sized TiO_2 feedstock particles, a porous microstructure has been developed which comprises pillars approximately 200 μm in height. These surfaces can be impregnated using various lubricating liquids/oils where the micro-pores can act as reservoirs. The resulting solid/oil interface is exceptionally slippery with a water contact angle hysteresis smaller than 2° which allows water droplets to slide on the surface with minimal energy dissipation. Icing tests in an icing wind tunnel have demonstrated icing mitigation, reduced ice adhesion and reasonable durability. Different types of oils with various properties have been used to determine the best performance and durability at different icing/deicing conditions. Additionally, confocal laser microscopy and scanning electron microscopy have been used to study the microstructure and microtexture of the coatings as well as oil penetration in the pores and oil depletion after coatings have been tested in icing conditions.

Acknowledgment

I would like to thank my academic supervisors Professor Ali Dolatabadi, Professor Christian Moreau and Professor Martin Pugh for their patient guidance, encouragement and advice they have provided throughout my time as a student, also for consistently pushing me forward and give me all the resources scientifically and financially to overcome all the obstacles and to continue my research and finish my thesis. I have been extremely lucky to have supervisors who cared so much about my work, and who responded to my questions and queries so promptly.

I must express my gratitude to all the Concordia University Thermal Spray Laboratory group members for all the help and encouragement during my work at Concordia University. Notably, the efforts of Dr. Fadhel Ben Ettouil, Dr. Navid Sharifi, Dr. Tahmine Forati, Khaled Yassin, Alexandre L, Maria, Ali N, Ali Z, Alex N, Fernanda C and Mohammad R in their assistance during experiments and in the preparation of experimental equipment is greatly appreciated.

Thanks are due to Concordia University's research staff, particularly Robert Oliver and Mazen Samara and administrative staff including Maureen Thuringer, Leslie Hosein, and Sophie Merineau.

This thesis work is dedicated to my wife, Farah, who has been a constant source of support and encouragement during the challenges of Master Studies and Life; I am truly thankful for having you in my life sweet angel.

I am forever indebted to my mom, Hana, my dad, Hyad and my brother Shoki for their unconditional love and ever-lasting support.

Table of Contents

List of Figures

List of Tables

List of Abbreviations

Abbreviation	*Meaning (unit)*
APS	Atmospheric Plasma Spray
SPS	Suspension Plasma Spray
CAH	Contact Angle Hysteresis (°)
SCA	Static Contact Angle (°)
ROA	Roll-Off Angle (°)
SA	Sliding Angle (°)
CLSM	Confocal Laser Scanning Microscopy
CVD	Chemical Vapor Deposition
PVD	Physical Vapor Deposition
DOE	Design of Experiments
HVOF	High Velocity Oxygen Fuel
HVAF	High Velocity Air Fuel
LFS	Liquid Flame Spray
IWT	Icing Wind Tunnel
PAA	Polyacrylic Acid
PTFE	Polytetrafluoroethylene
PPy	Polypyrrole
BMLm	1-butyl-3-methylimidazolium bis (trifluoromethylsulfonyl) imide
LIS	lubricant-infused surfaces

OTS	Octadecyltrichlorosilane
LCFS	Laser Confocal Fluorescence Microscopy
RCA	Receding Contact Angle (°)
SA	Sliding Angle (°)
SEM	Scanning Electron Microscopy
LWC	Liquid Water Content (g/m^3)

Chapter 1. Introduction

Airplane manufacturing is one of the most sophisticated and advanced industries in the modern era. However, there are many challenges related to maintaining the aircraft's performance in flight where the temperature decreases which can result in ice accumulation on the wing. This will increase the drag force, which will cause the airplane to lose airspeed and lift, forcing the pilot to increase the engine power and "fuel consumption", in order to maintain the correct amount of lift. Additionally, ice will increase the weight and thus decrease the lift, forcing the airplane to lose altitude.

Generally, there are two types of ice generated on aerodynamic components; Glaze and Rime ice [1]. Glaze or clear ice, is dense and transparent and appears when the water droplet has sufficient time to hit the airfoil and spread on its surface, covering more areas. At low temperature, the distributed water will freeze and create a transparent layer that it is not easy to observe from inside the plane: it can also fill all the voids on the surface, which gives it a high attachment strength and will not detached easily. This type of ice is dangerous and harmful.

Rime ice is translucent or opaque and brittle because it contains in its microstructure many air pockets (pores) which make it less dense than Glaze ice. Rime ice forms immediately after the impact of the droplet, meaning the droplet doesn't have much time to run back over the airfoil and it can be seen as white ice on/near the leading edge of the airfoil.

Droplet size, air temperature and liquid water content are factors that are important in icing type. Glaze and Rime ice are illustrated in Figure 1-1.

Figure 1-1 a) Glaze ice b) Rime ice [1].

1.1 Motivation

In 1994, an airplane crashed in Roselawn-Indiana, taking the lives of 68 passengers on board. According to The National Transportation Safety Board (NTSB) [2], they determined that the probable causes of this accident was loss of control, attributed to a sudden ice-accumulation on the deicer boots (the front part of the airfoil) shown in Figure 1-2, which eventually led to loss of control and the crash.

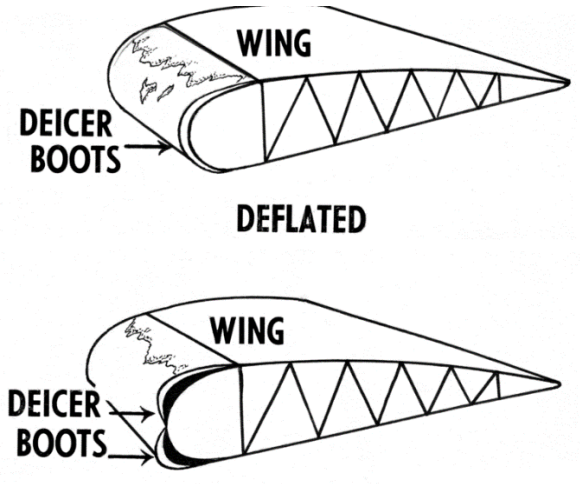

Figure 1-2. Deicer Boots inflated and deflated [3].

Many accidents have occurred during the past 30 years related to icing problems [4] e.g.:

- Continental Airlines Inc. Accident in Denver, Colorado in 1987 with 28 fatalities.

- US AIR INC. Accident in Flushing, New York in 1992 with 27 fatalities.
- Embraer EMB – 120RT Accident in Monroe, Michigan in 1997 with 29 fatalities.

As a result of all these incidents, numerous efforts have been made to closely study the icing phenomenon and the reason behind it and how to prevent future accidents. Different techniques have been developed (mechanical, chemical, and thermal) for deicing systems.

1.1.1 Mechanical Deicing

Basically, it is about breaking the bond between the ice particles and the wing surface thus removing it from the surface. This technique uses a semi rubber balloon which can be inflated with air (as shown schematically in Figure 1-2) with the help of a compressor and, by this inflation process, it can break off the ice as long as it is within a certain thickness and width. Of course, the drawback of this technique is it can only be applied on small airplanes [3].

1.1.2 Chemical Deicing

Chemical deicing uses a liquid that can integrate with water droplets and prevent them from freezing, in other words, preventing the bond between the ice and the surface rather than breaking it. Different materials can be used for anti-icing e.g. potassium acetate and potassium format. However, this process is practically only used for ground anti-icing, especially in airports during ice storms. The practical temperature limit is (-32°C) [5].

1.1.3 Thermal Deicing

A common thermal deicing system is one that uses electrical heating elements that with a certain electrical power can heat up and melt the ice on top of the element. Various materials with different techniques have been used to heat up critical components such as aircraft wings and engine nacelles [6]. In addition, there is a different approach where some of the heat from the exhaust system of the turbine engine is redirected to melt the ice by guiding tubes [7], as shown in Figure 1-3.

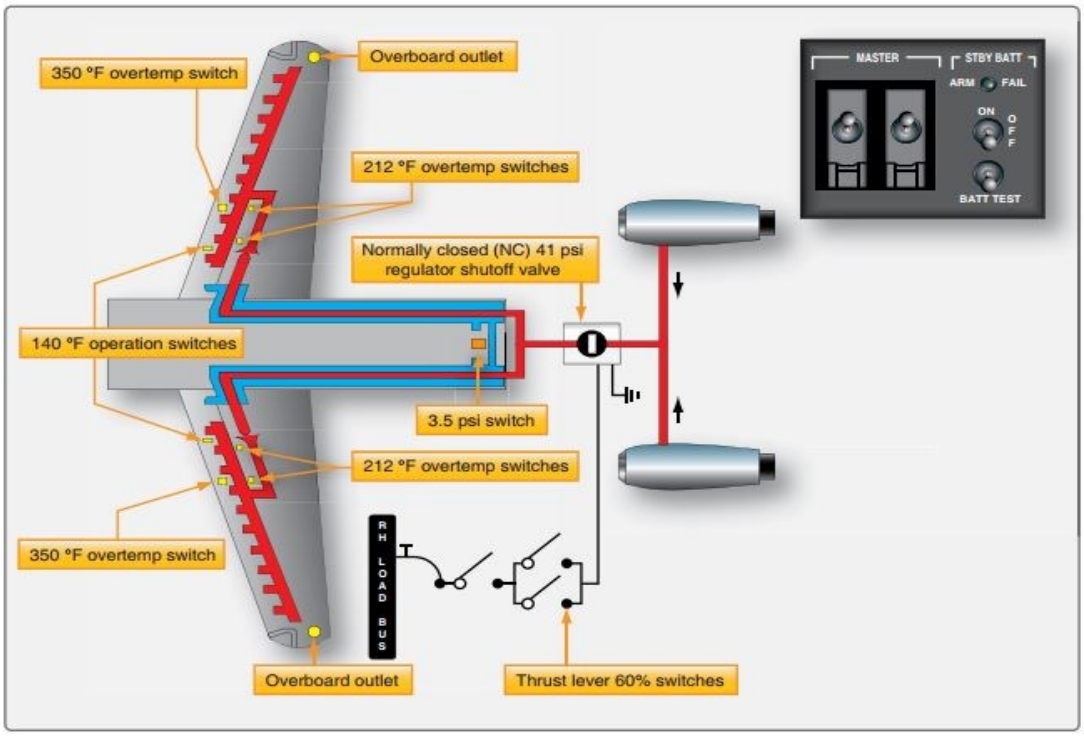

Figure 1-3. A typical ice protection system schematic for a business jet [7].

1.1.4 Surface modification and anti-icing surfaces

A different approach to avoid ice-accumulation is by preventing the super-cooled droplet of water from sticking to the surface, in other words, delaying ice build-up or facilitating its removal. This approach can be done by understanding the formation of ice on a surface, static contact angle (SCA) and contact angle hysteresis (CAH) that can affect the freezing process. These values are the main parameters that should be controlled to achieve the best results, and all this can be done by choosing the correct coating material and correct techniques that can give the best result in producing a *phobic-to-ice* surface.

One way to reduce ice adhesion is to use a superhydrophobic surface. Ideally smooth surfaces can have a certain amount of hydrophobicity due to their surface's chemistry, however superhydrophobicity comes from the microtexture or nanotexture of the surface which can increase water repellency. Furthermore, developing a hierarchical texture, which means having two scales of roughness on the surface, can provide the best water repelling characteristics. In this case air pockets are created between the material surface and the water, therefore providing the superhydrophobicity and this is seen on "**natural superhydrophobic surfaces**" such as the lotus

leaf on which there are micro sized nodes/ bumps and these bumps create the micro-scale roughness. Figure 1-4 illustrates this surface texture effect. Adding to this superhydrophobicity effect, there is a technology known as Slippery Liquid-Infused Porous Surfaces (SLIPS), which has a low mobility in terms of contact angle hysteresis. This technique depends on infusing a lubricant with a specific property into a micro or nano surface structure which creates the needed slippery surface. In the current research, creating SLIPS depends on having a superhydrophobic surface as its base layer. In the up-coming chapters the author will explain more about this technique.

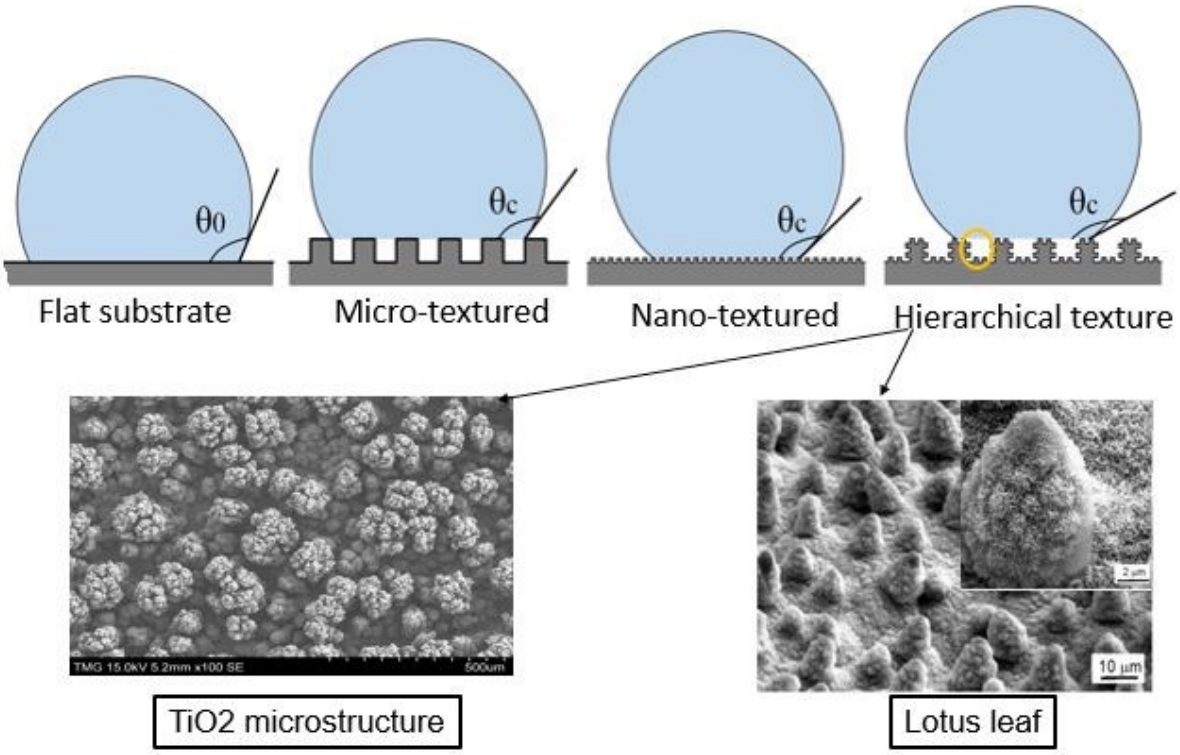

Figure 1-4. Surface texture, natural and artificial [8].

Superhydrophobicity is the combination of low surface energy and specific surface morphology. There are a good number of commercial superhydrophobic coatings that rely primarily on producing a low surface energy. These are usually polymeric/organic materials but the problem with them is that they have poor mechanical properties especially in the case of icing/deicing. On the other hand, those surfaces that rely only on the surface morphology (complex coating/ vacuum based processes) are complex with a high cost and they are hardly scalable insomuch as they are difficult to apply on large surfaces. Furthermore, the goal of our research is

to develop a method that can provide superhydrophobicity and then impregnate such a surface with a lubricant oil so that to bring the preferred features – water-repellency, low cost, scalability and durability – together.

1.1.5 Thermal Spraying

Many techniques can be used in order to build-up a coating layer on top of a surface. The list includes: Physical Vapour Deposition (PVD), Chemical Vapour Deposition (CVD), Vacuum Cold Spray, High Velocity Oxygen Fuel (HVOF), High Velocity Air Fuel (HVAF), Atmospheric Plasma Spray (APS), Suspension Plasma Spray (SPS), etc. Of these, APS and SPS are the ones most commonly used to produce a coating layer with micron or submicron texture. Figure 1-5 shows a schematic of a plasma spray system. Depending on the system, the feedstock can be either a liquid-powder suspension (SPS) or solid powder (APS). Both of these techniques provide a coating with high quality in terms of mechanical properties, durability and scalability [8].

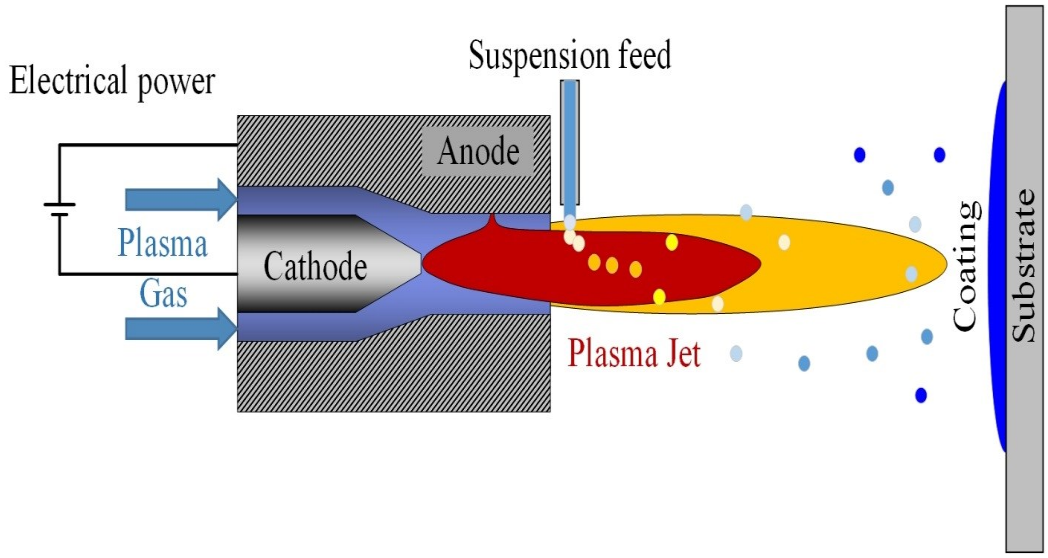

Figure 1-5. A schematic of suspension plasma spray technique [8].

1.2 Rational for proposed work

Most of the recent studies on anti-icing and water-repelling surfaces focus on using fluoropolymer-based materials, and they give a very good results in terms of Static Contact Angle (CA) and Sliding Angle (SA), but the main disadvantage of these materials is that they have low durability. In other words, the coatings cannot withstand harsh conditions for a long period of time.

As mentioned above, another approach has been used to create a hard, wear-resistant surface microstructure that can act as an oil reservoir which can keep the oil between its pillars and feed the substrate's surface with oil, creating what is called a Slippery Liquid Infused Porous Surface (SLIPS). This can be created by using different techniques, for example, Lithography techniques were used to create such a surface on patterned silicon substrate [9], whereas a different approach used Liquid Flame Spray (LFS) [10] and another used a Photolithography technique which involved transferring a pattern with a very small size (micro/nano) scale onto a substrate [11]. Adding to what has been mentioned, some researchers tried electro-deposition of highly textured Polypyrrole (PPy) on aluminum substrates followed by fluorination of the structured coating and infiltration with the lubricant [12]. The above-mentioned techniques produced good results with regard to low CAH and SA values but the disadvantage of these techniques is that they are expensive, time consuming and not easy to apply on large scale parts.

Starting from that point, the author worked in this research on developing the desired microstructure with practical techniques that can be scalable, time saving with an acceptable cost and can provide good mechanical properties and durability. To conclude, the purpose of the current work is to develop a technique using the SPS technique with specific parameters and selecting an appropriate oil with properties that can achieve a low CAH and SA with longer durability than fluoropolymer coatings under realistic flight conditions.

1.3 Objectives

The main objectives of this research are presented here with respect to the sequence of the chapters of this thesis:

- Developing a hierarchical microtexture on the substrate's surface with two scales of roughness using Suspension Plasma Spray.
- Impregnating this surface structure with an appropriate oil and studying its behavior.
- Testing the mobility and icing performance of the coated substrate in an icing wind tunnel.

1.4 Thesis Outline

In the first chapter, the author introduced the problem by explaining the types of ice and how it can affect the airfoils of aircrafts. Following a brief summary of the deadly impact of the

icing problem, the author addressed the techniques that have been used to overcome the icing problem.

Chapter 2, explains the physical analysis of the static contact angle (SCA) and contact angle hysteresis (CAH), also defines the concepts of superhydrophobicity and surface roughness and adding to that, the oil impregnation techniques and the measurements that can be extracted from it. Furthermore, the two thermal spraying processes that have been used in this research; atmospheric plasma spraying (APS) and suspension plasma spraying (SPS) are explained.

In Chapter 3, the author explains the materials that have been used and the experimental procedure that has been followed, from preparing the substrates, through coating deposition until the collection of experimental data in icing conditions.

In Chapter 4, the author presents the analyzed data in the form of tables and figures and discusses the results in a manner that outlines a solution to the icing problem and whether it has sufficient durability.

Chapter 5 summarizes the findings, conclusions and contributions of this work and suggests some recommendations for future work.

Chapter 2. Literature Review

This chapter will provide a well explanation about the young's equation and the concept behind the wettability and mobility of a liquid droplet. The definition of superhydrophobicity, the oil impregnation techniques and the study cases that have been carried out. Along with the thermal spraying process and the techniques that have been used in this research. Finally, the challenges that accompany this technique are discussed.

2.1 Contact Angle: Young's Equation

Wettability is the ability of a liquid droplet to wet a surface. In other words, it is the interface between solid, liquid and gas phases. Mobility, is the ability of a droplet to move easily on a surface. Measuring the mobility parameters is an important factor, because it plays a key role in many applications e.g. anti-icing, anti-fouling, so called self-cleaning, etc. Wettability and mobility can be defined with the following parameters: *Static contact angle* (SCA), *contact angle Hysteresis* (CAH) and finally *Sliding angle* (SA).

Static contact angle (SCA) represents the degree of wetting when a solid and liquid interact whereby a small contact angle ($\theta_c < 90°$) corresponds to a high degree of wettability (the droplet will spread and wet the surface). A surface with this characteristic is known as a hydrophilic surface, whereas one that gives a high contact angle ($\theta_c > 90°$) is referred to as a hydrophobic surface and corresponds to a low degree of wettability. When the contact angle is very high (θ_c >150°) the surface is described as being *superhydrophobic* with an extremely high water repellency. Thomas Young [13] was the first to describe the contact angle of a liquid droplet on a solid surface, which defines the effect of the three interfacial tensions by Equation. (2.1):

$$\gamma_{lv} \cos\theta_Y = \gamma_{sv} - \gamma_{sl} \qquad \text{Eq. (2.1)}$$

where θ_Y is Young's contact angle, while γ_{lv}, γ_{sv} and γ_{sl} represent the liquid-vapor, solid-vapor and solid-liquid interfacial tensions. This equation is usually known as Young's equation. A schematic of different contact angles is shown in Figure 2-1 [14].

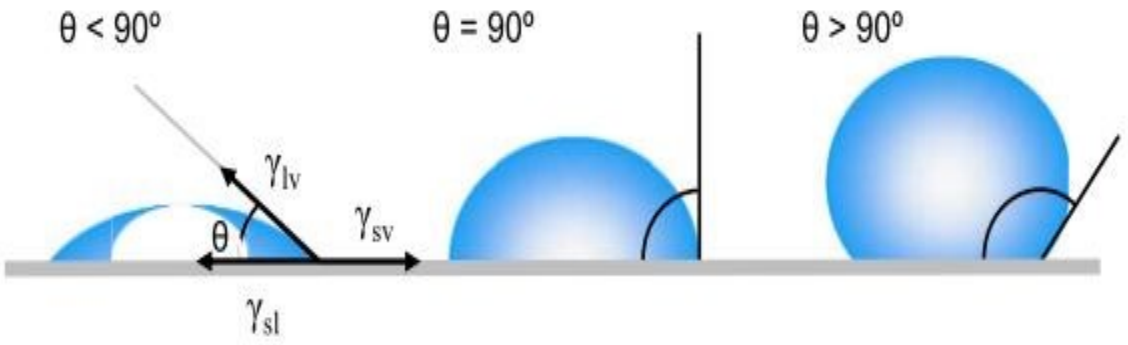

Figure 2-1. Schematic of different contact angles of a liquid droplet on a solid surface.

2.2 Contact Angle Hysteresis (CAH) and Sliding Angle (SA)

The static contact angle represents the wettability measurements made in a static state, but from a realistic point of view the situation is usually not static and we need to study dynamic contact angles, that is to say the mobility of the droplet on the surface [15]. This is known as the *Contact angle Hysteresis* (CAH), and is the difference between the advancing contact angle, θ_a, (measured during expansion of a liquid droplet) and the receding angle, θ_r, (measured during contraction of the droplet) as shown schematically in Figure 2-2. The CAH can be related to the energy dissipation that occurs during the movement of a droplet on the surface and the CAH is given by Equation. (2.2):

$$CAH = \theta_a - \theta_r \qquad \text{Eq. (2.2)}$$

Depending on the CAH values, the liquid droplet will act accordingly: water droplets with a low CAH (less than 10°) will move easily on a surface while droplets with high CAH will tend to stick on the surfaces and not move easily.

In addition to *Contact angle Hysteresis* another parameter should be taken into consideration which is the *Sliding angle* (SA). This represents the angle at which a surface has to be tilted in order for the droplet to start sliding on the surface, denoted here as θ_S. SA and CAH tends to be correlated as the both characterize the dynamic wetting behavior of a water droplet on a surface. Water repellant surfaces with both SA and CAH <10° are likely to known as superhydrophobic surfaces with excellent water mobility features, leading to a delay in ice build-up and facilitating its removal. In other words, when the liquid droplet impinges onto the superhydrophobic surface minimal contact will occur between the liquid and solid interface allowing the droplet to slide on the surface at a minimum tilting force leading to a delay in the occurrence of ice. "However, it is important to note that the values of contact angle hysteresis and sliding angle are not necessarily the same" [16].

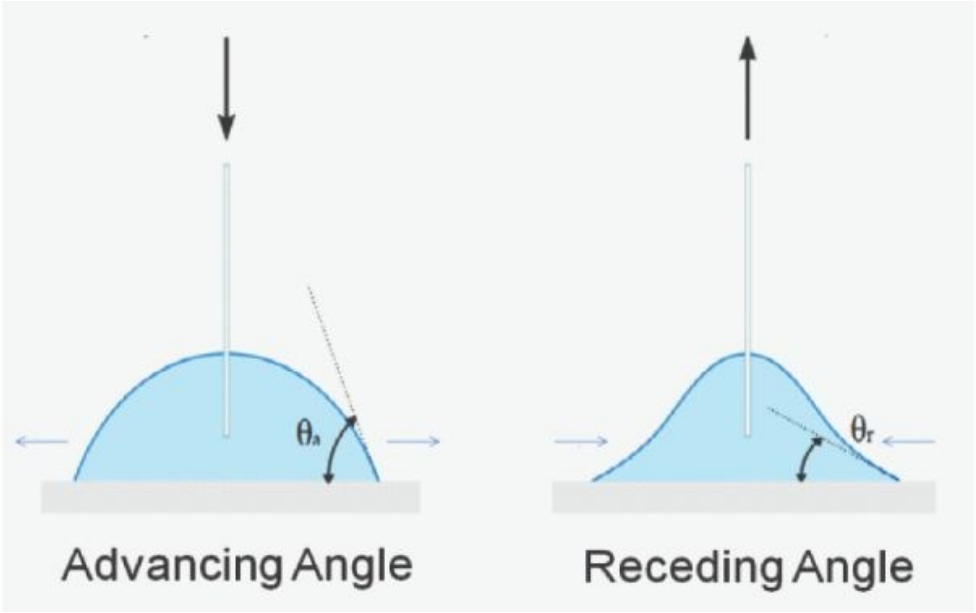

(a) (b)

Figure 2-2. Schematic of a static contact angle degree between (a) advancing angle and (b) receding angle.

2.3 Superhydrophobicity and Surface Roughness

The development of superhydrophobic surfaces have been inspired by nature, for example; the lotus leaf, water strider insects and penguin feathers. The scientific reason for their hydrophobicity is due to their surface's chemistry and their surface morphology that is composed

of micro and nano nodes, meaning there are two scales of roughness on the surface. There is also the presence of biological epicuticular wax which has a low surface energy. Together, these features can provide excellent water-repellent characteristics, which creates air pockets between the surface and the water therefore providing the hydrophobicity.

There are two regimes that have been used to clarify the effect of surface roughness and surface energy. The first is known as the Wenzel regime [17], or *homogeneous wetting*. In this case the liquid droplet can penetrate the gaps between the micro-pillars on the surface. By lowering the surface energy and increasing the surface roughness, air-pockets can be produced which act as cushions separating the solid and the liquid interfaces (giving a composite interface) and this is described by the Cassie-Baxter model [18] - heterogeneous wetting as shown in Figure 2-3. Note that, the difference between surface tension and surface energy, is that the first measure the applied force along a line whereas the second measure the energy along an area, in this research the focus is on the surface energy.

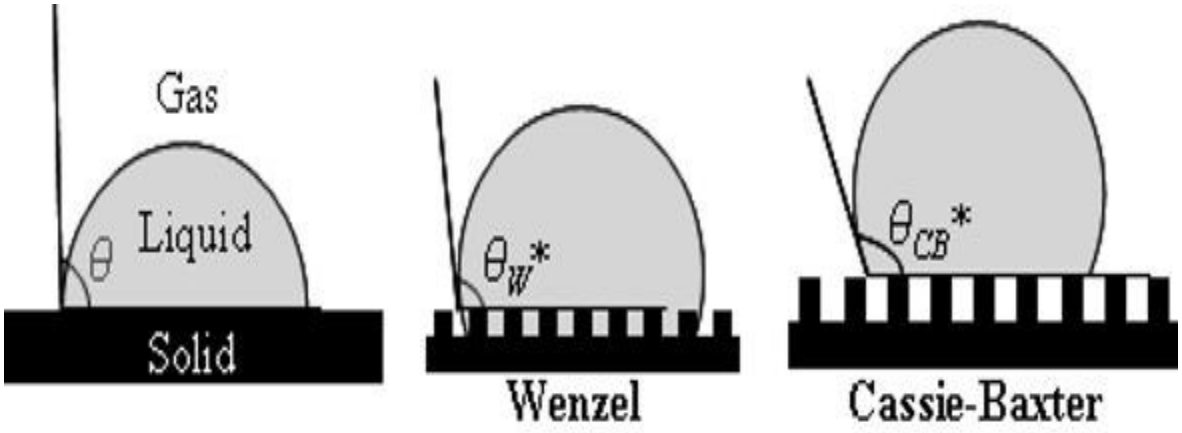

Figure 2-3. Schematic of Wenzel and Cassie-Baxter models. [18]

Note that the difference between surface tension and surface energy is that the first is measured along a line while the second measured along an area, in the research we will be talking about lowering the surface energy to create the superhydrophobic surface. Furthermore, in the Wenzel model, the liquid droplet will penetrate between the micro-pillars until it reaches the surface. At that moment, the adhesion between the liquid and solid will be high which eventually will decrease

the water mobility on the surface, and this explains why *hydrophilic* surfaces have a low water mobility. On the other hand, in the Cassie-Baxter model, the surface tends to be *hydrophobic* and will produce a surface with higher water repellency. Studies have shown [8] that having an hierarchical roughness texture (for example, a dual scale roughness at the nano and micro levels) can have promising properties with high contact angles (SCA>150°) and high mobility of the droplet on the surface (SA<10°). This is why the author has focused on having a hierarchical texture to create the initial hydrophobicity as illustrated in Figure 2-4. Thermal spraying is a promising technique that can produce such a hierarchical texture which is the starting material for the liquid infused surfaces under investigation in the present study will be discussed later.

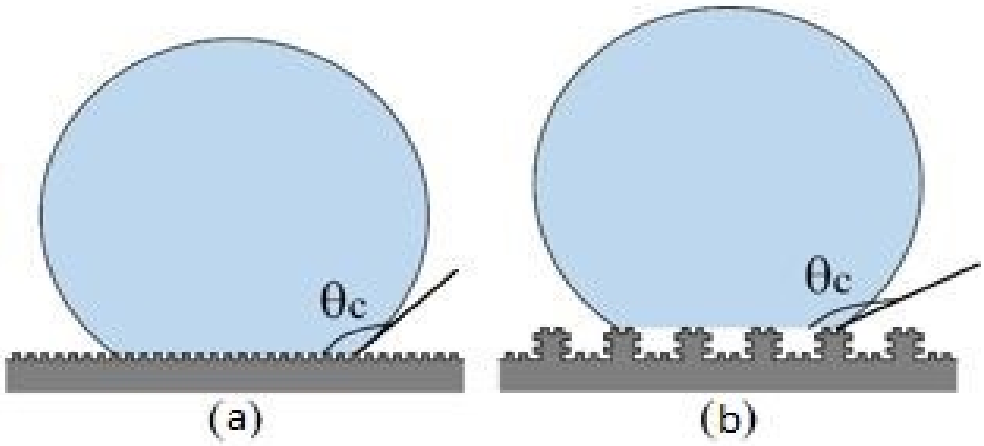

Figure 2-4. Schematic for wetting of (a) nano-texture and (b) hierarchical texture. [19]

2.4 Slippery Liquid Infused Porous Surfaces (SLIPS)

Superhydrophobic surfaces have numerous promising applications, e.g. anti-icing, anti-fogging and self-cleaning surfaces [9]. As discussed previously, superhydrophobicity can be created from the trapped air-pockets between micro and nano pillars. Furthermore, preserving the pockets in place is a challenging process due to many factors that may make them collapse, e.g.

applying of a high pressure can force liquid into the surface and take the place of the gas phase [20], and mechanical damage occurring to the micro or nano texture can affect the mobility results and significantly decrease droplet mobility [21]. Furthermore, condensation or ice-nucleation can appear on the nano texture and replace the gas phase which will also affect the superhydrophobicity [22].

In order to overcome the previous challenges, a new approach has been used to infuse liquid into the surface layer and replace the gas-phase to produce what is known as Slippery Liquid Infused Porous Surfaces (SLIPS). The liquid introduced is a lubricating fluid with a certain viscosity that it is higher than the liquid to be repelled (in our case the water droplet). Generally speaking, these two liquids, lubricant and water, are immiscible which prevents mixing. Finally, having a lubricating liquid which is incompressible, but mobile, is the main advantage of SLIPS, as the lubricant can remain in place even when a high wetting pressure is applied to the surface but also can flow to allow self-repair of the surface if damage due to scratches, abrasion, icing, etc.

2.4.1 Oil Impregnation Techniques

Recently, some workers have developed SLIPS by using magnetic fields [23]. This type of material can have superhydrophobic surfaces at very low temperatures (-34°C) with a low ice adhesion strength of approximately 2 Pa. It can also be applied to any surface without modifying the structure of the surface at (the nano- and micro-scale). The concept behind this technique depends on having a ferrofluid which is a colloidal mixture of a liquid (usually an organic solvent or water) with ferromagnetic nanoparticles that can be affected with a magnetic field. The solvent should have a low evaporation rate in order not to be evaporated when magnetized.

Ice accumulation usually results when a liquid droplet hits the substrate surface creating a solid-liquid interface with a *high-energy interface* which will allow the ice to build-up, but in this ferrofluidic study, as soon as the droplet hits the oil layer it will penetrate it, as it can be seen in Figure 2-5. a. As soon as the magnetic field is activated, it will create shock waves as a result of the Ferrofluid behavior\, causing the droplet of water to be pushed up, creating a liquid-liquid interface which doesn't allow easy formation of ice due to it being a *low-energy interface*. The magnetic field strength controls the amplitude of the wave as shown Figure 2-5. b.

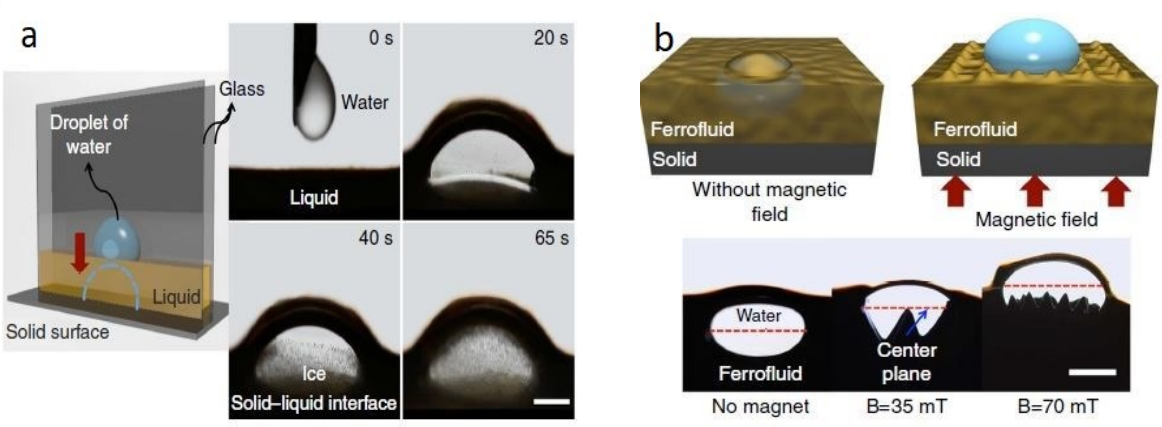

Figure 2-5. (a) Water droplet penetrating the oil layer to create a solid-liquid interface (b) How the water droplet reacts when the magnetic field is on [23].

The main disadvantage of this technique is that it is very complex and predicting the magnetic field behavior is not an easy task.

Other studies have shown that applying an oil-impregnation process to an existing superhydrophobic surface can improve the efficiency of removing water droplets [12]. Instead of creating a surface with high texture (nano-micro texture), the researchers developed their coating on a smooth surface which gave very low mobility results in a high-humidity environment as can be seen in Figure 2-6. The basis of this process is to have an organic conducting polymer, *Polypyrrole* (PPy) that can be coated on an Al sheet by electrodeposition and then by controlling the current and time of the process they can control the morphology at the nanometer scale. Furthermore, they added fluorine to the coating in order to improve the high-binding energy and resistance of the plastic. Finally, they infused a low-viscosity perfluorinated lubricating fluid. In applications where there are low vibration effects and low pressure, oils with low viscosity present a good option to create SLIPS with a thin layer impregnated in a nano-textured surface. The advantages of this technique are that it is scalable, can be applied on large scale components, can be applied on complex shapes, does not produce toxic vapors and the polypyrrole itself is an anti-corrosive material. The disadvantages of electrodeposition are that creating a uniform plating is challenging and the process is costly and time consuming and there is always a possibility for pollution.

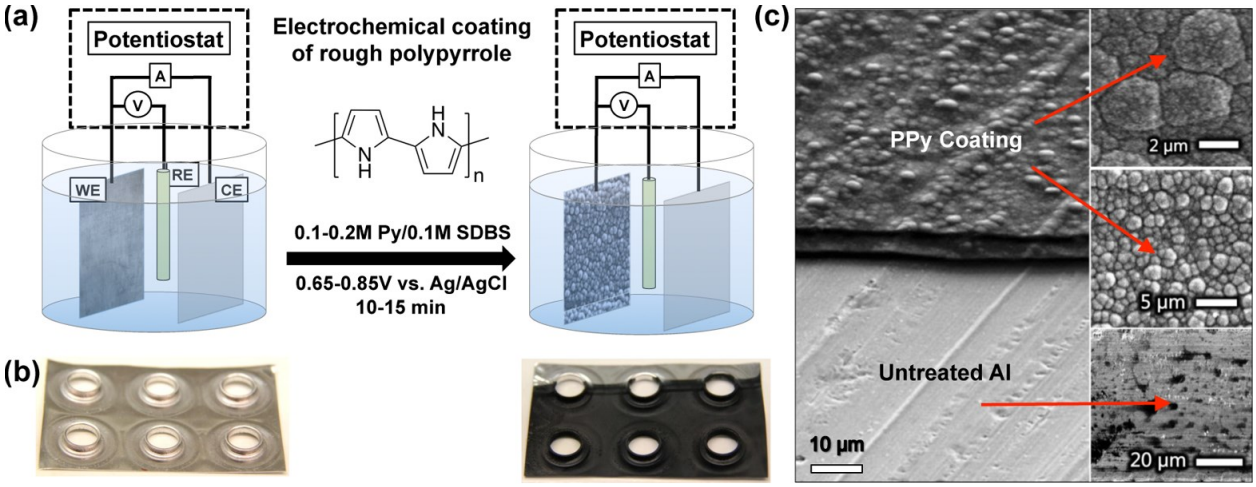

Figure 2-6. (a) Schematic of the electro-deposition process on an Al sheet (b) Al sheet before and after coating (c) SEM images of the PPy coating. [12]

Regarding the production of suitable surfaces, some researchers [24] used a smooth polytetrafluoroethylene (PTFE) sheet which was grit blasted to create a textured surface, then different types of lubricating fluids were applied to finally create a lubricant-infused surface (LIS).

Additionally, other researchers have developed a microtexture with a lithographically patterned silicon micropost array coated with OTS (octadecyltrichlorosilane) [9] as shown in Figure 2-7. Then they lowered the surface energy by a post-treatment using silane, and finally applied the lubricant oil which was silicone oil or a non-water-soluble ionic liquid.

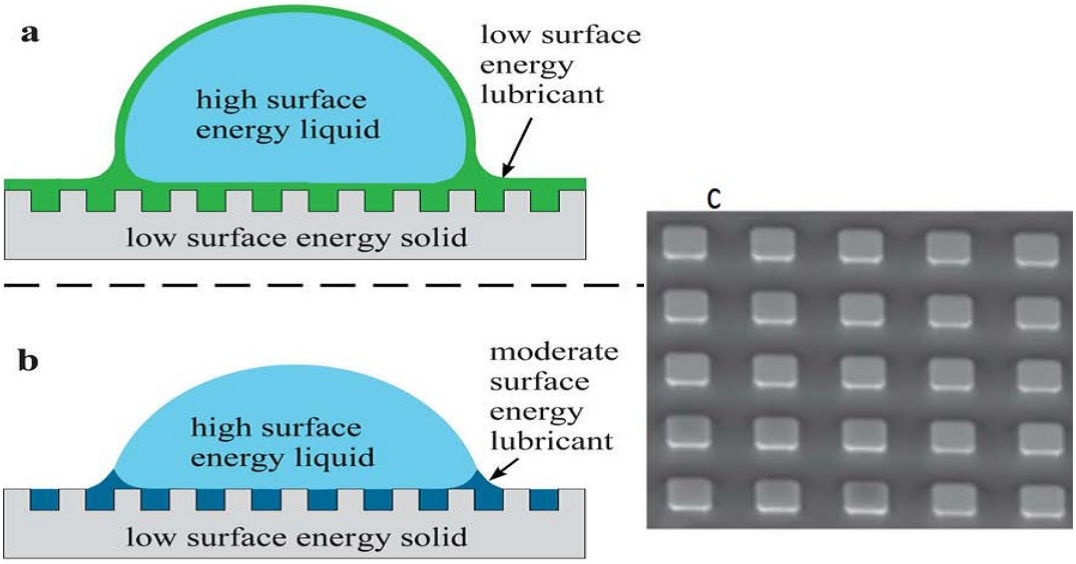

Figure 2-7. Schematic diagram of a liquid droplet (a) cloaked in a lubricant oil (b) floating on the lubricant (c) an LCFM image of the patterned micro texture [9].

Another promising technique is *Liquid Flame Spray* (LFS). It has been used to develop a nanotexture of TiO2 on a low-density polyethylene film which then had silicone oil applied to achieve the needed SLIPS, as can be seen in Figure 2-8 [10].

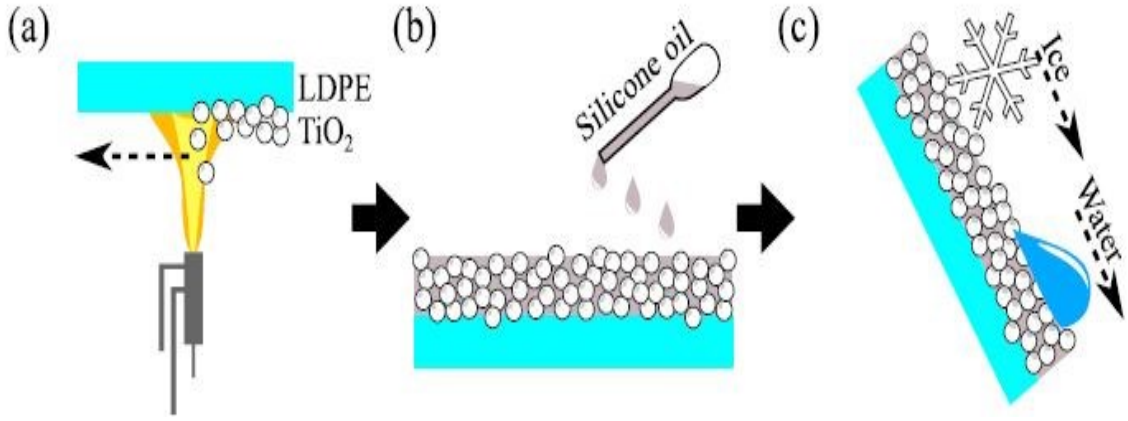

Figure 2-8. Schematic diagram of (a) Thermal spraying the nano particles (b) oil impregnation (c) mobility measurements [10].

Geyunjian et al introduced a fast and easy method to develop SLIPS by applying Layer-by-Layer (LBL) polyelectrolyte assembly in an organic solvent as illustrated in Figure 2-9.

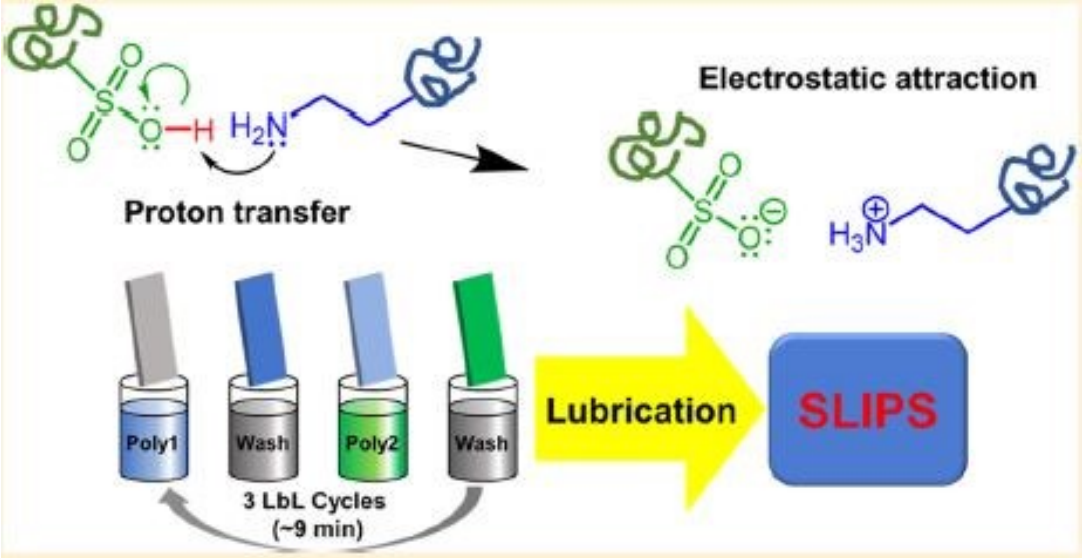

Figure 2-9. Shows a schematic of the proton transfer mechanism from Sulfonic Acid to Amine group resulting in electrostatic attraction [25].

By controlling the LBL assembly parameters including dipping cycles, dipping time, drying time between one cycle and another, they were able to produce the polyelectrolyte with different thickness which is the base porous structure. Finally they used the oil-infusion process to create the needed SLIPS [25].

Wei Ma et al. [26], introduced a hydrothermal method in which a perfluoropolyether lubricating (PFPE) liquid is infused into a nano-textured alumina gel film that was modified with perfluoroalkyl-phosphonic acid to create the needed SLIPS. The purpose was to apply the SLIPS process with optical transparency. The nano-textured surface was obtained by hydrothermal synthesis of the sol-gel structure and the cauliflower-like structure was produced as in Figure 2-10 followed by liquid infusion of the PFPE.

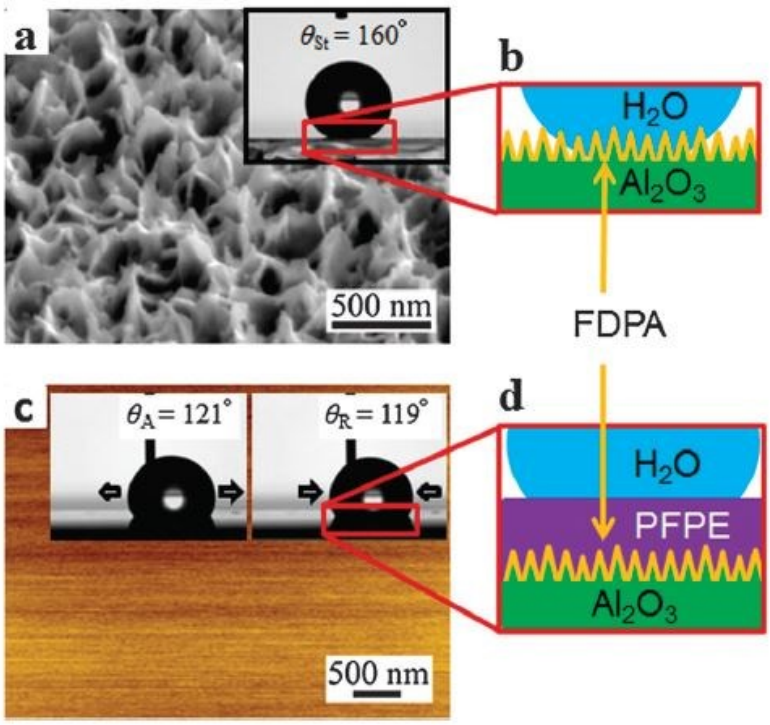

Figure 2-10. a) SEM image of the nanotexture with static contact angle b) Schematic of the interaction between liquid, oil, and solid, c) Contact angle hysteresis d) Schematic of the interaction between liquid, oil, PFPE and solid [26].

Jing Wang et al. [27] were successful in producing SLIPS on a wide range of materials (stainless steel 304/316, carbon steel, titanium, aluminum, copper, glass and ceramics) where the surface nano-texture was obtained by appropriate chemical etching (e.g. hydrochloric acid, ferric chloride acid and boiling sodium bicarbonate solution) after which a silanization process was carried out for a certain time in order to modify the surface morphology. After evaporating the excess silane an oil-impregnation process was performed using perfluorinated oils by spraying or spin coating. The main feature of this technique is surface damage can be healed by thermal-repair using oxygen plasma between 120 to 200 °C. The difference between treated and unhealed surfaces are demonstrated in Figure 2-11.

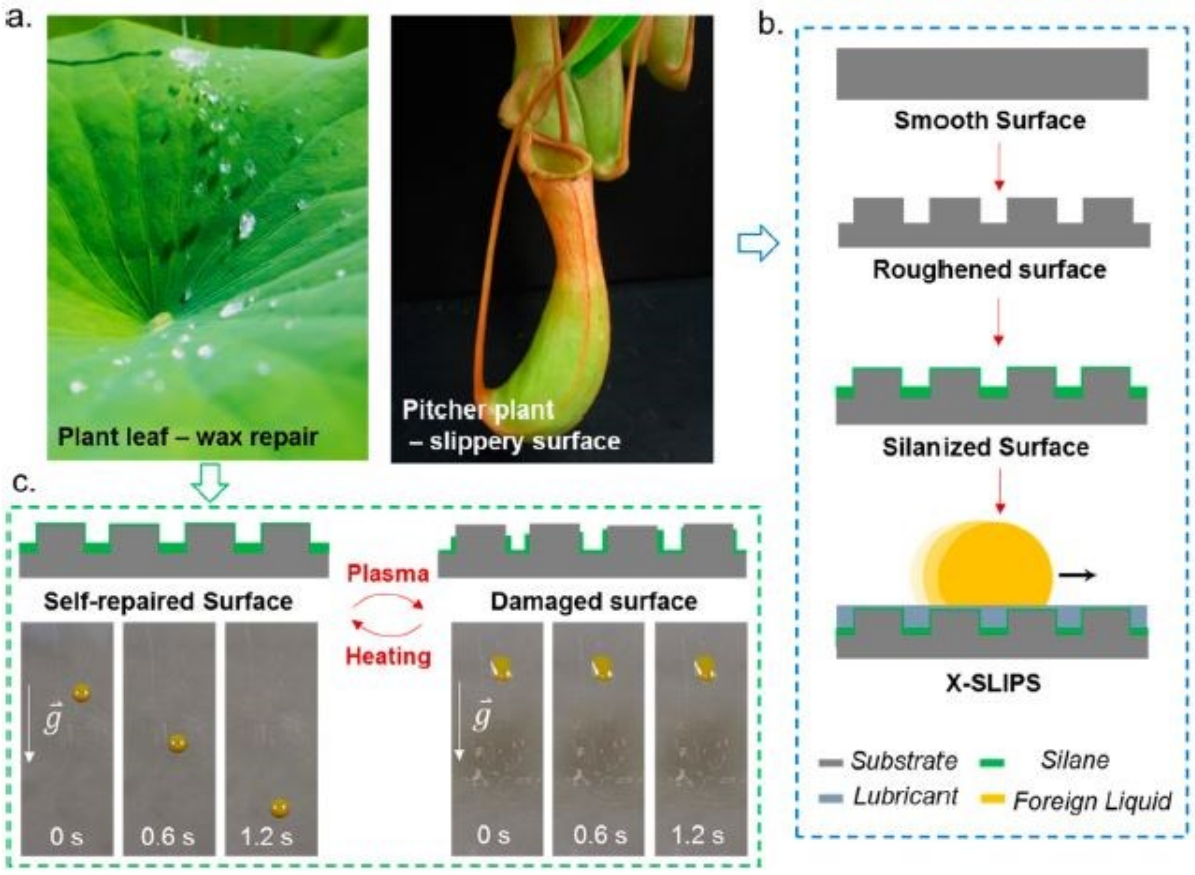

Figure 2-11. Shows a) Natural superhydrophobic and Slips plants b) Schematic of the nano/micro structure c) Difference between damaged and healed surface [27].

2.4.2 Characteristics and Performance of SLIPS

In the sections above some of the techniques for developing the required surface texture and oil impregnation have been discussed: in this section the focus will be on the characteristics of SLIPS surfaces.

A study was carried out by K. Philseok et al. [12], to study *the contact angle hysteresis* (CAH) and *the critical diameter of a liquid droplet* (D_c) on different SLIPS surfaces by applying lubricant oils with a wide range of viscosities. The critical diameter is calculated as follows in Equation. (2.3) and denotes the minimum diameter of a droplet at which sliding begins:

$$D_c = \left(\frac{24sin^3\theta_A\gamma(cos\theta_R - cos\theta_A)}{\pi\rho(1-cos\theta_A)^2(2+cos\theta_A)gsin\alpha}\right)^{\frac{1}{2}} \qquad \text{Eq. (2.3)}$$

ρ is the density of water, g is the standard acceleration due to gravity, α is the tilting angle, γ is the surface tension of water, and θ_A and θ_R are the advancing contact angle and the receding contact angle respectively. After measuring D_c on a SLIPS-Al sheet and a bare Al sheet they found that D_c on the SLIPS surface is 8 times smaller than the bare one thus more droplets are repelled, and this is due to the presence of the lubricating oil.

Other researchers including Jeong-Hyun et al. [24], focused their study on the role of the viscosity ratio between water and the oil. The study was carried out by measuring the impact time of a liquid droplet on SLIPS impregnated with various oils. The Weber number at impact was the key parameter that has to be considered, as it can be seen in Equation, (2.4):

$$We = \frac{\rho_w U_{0D_o}^2}{\gamma_w} \qquad \text{Eq. (2.4)}$$

ρ_w is the density of the droplet, U_o is the drop impact velocity, D_o is the initial diameter of the droplet before impact, and γ_w is the surface tension of the droplet. The results showed that the impact time might vary according to low and high Weber number and also it depends on the substrate's surface properties, whether it is hydrophobic or superhydrophobic. A key finding was the importance of having a high ratio of viscosity between the droplet and the infused oil, where they conclude that at all We numbers, the maximum spreading diameter increased with decreasing the oil's viscosity.

According to J. David smith et al. [9], there several factors that control droplet shedding between a liquid droplet and the lubricant oil. Usually the oil viscosity is the key parameter that can define how the droplet will be shed as can be seen in Figure 2-12. The authors give 12 scenarios in which the droplet can act. The spreading coefficient can define the criterion for cloaking (whereby the droplet is totally encapsulated by the oil film) as can be seen in Equation. (2.5):

$$S_{ow(a)} = \gamma_{wa} - \gamma_{wo} - \gamma_{oa} \qquad \text{Eq. (2.5)}$$

Where γ_{wa} the surface tension between water, air interfaces, γ_{wo} the surface tension between water, oil interfaces and finally γ_{oa} is the surface tension between oil and air interfaces. The results shows that the lubricant oil will cloak the water droplet when $S_{ow(a)} > 0$ and the oil will surround it only partially at the water-oil-solid interface when $S_{ow(a)} < 0$.

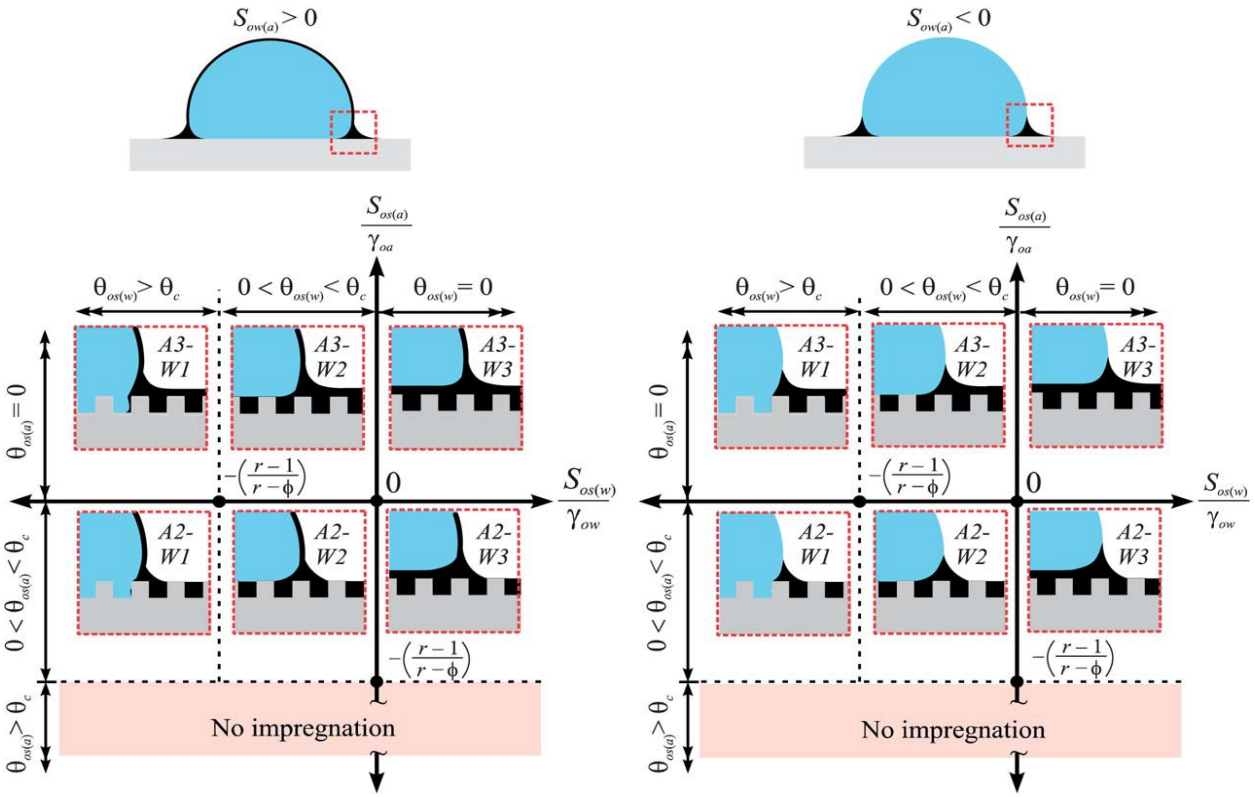

Figure 2-12. Schematic shows whether the liquid droplet will cloaked or not by the lubricant oil [9].

A recent study has been done by P. Juuti et al. [10], in which they developed a micro texture with Liquid Flame Spray (LFS) and, after applying an oil impregnation process, an ice-adhesion test was carried out. They built the ice layer in a wind tunnel at a temperature -10°C and with an air velocity of 25 m/s. The data that they collected to measure *the shear stress* (τ) showed an ice adhesion strength less than 25 KPa compared to 250 KPa for a LFS coated sample with no oil impregnation. The Equation. (2.6) is *the shear stress* (τ):

$$\tau = \frac{F}{A} = \frac{mr\omega^2}{A} = \frac{mr(\alpha t)^2}{A} \qquad \text{Eq. (2.6)}$$

F is the centrifugal force required to detach the ice from the sample's surface, A is the contact surface area, m is the ice accumulated mass, α is the constant angular acceleration and finally t is detachment time.

As previously mentioned, there are many oil impregnation techniques and more are being developed. In this research we focus on optimizing the process for anti-icing applications, where very harsh environment conditions occur. The techniques mentioned above have their limitations. Some have low mechanical properties and poor durability, whilst others are very complex and are

not scalable, in other words can't be applied on large scale components. In this research, we focus on two main things; firstly, having a hierarchical structure wherein 2 scales of roughness exist which can withstand harsh conditions and preserve the needed mechanical properties, and secondly on being able to produce oil impregnation that can provide the best mobility results. This can be achieved using a thermal spray processes to produce the needed coatings. In the next section, Atmospheric Plasma Spray (APS) and Suspension Plasma Spray (SPS) techniques are briefly presented, followed by the challenges that accompany these techniques.

2.5 Thermal Spray Processes

2.5.1 Atmospheric Plasma Spray (APS)

Atmospheric Plasma Spray (APS) is a process in which particles with a certain size that can be metals, ceramics and composites are heated by a plasma and then deposited onto a substrate surface in order to build up the coating layer. These particles are usually in the form of a fine powder which are injected into a very high temperature plasma plume, and rapidly gain a high temperature and are accelerated to a high velocity toward the target. Then the hot particles or droplets impact on the substrate surface and cool rapidly, forming a coating layer with interesting mechanical and physical properties [28].

The APS process comprises a high intensity DC current arc between an anode and cathode that will ionize the gas flowing between the electrodes that produces a plasma jet within the plasma torch. Both the cathode and anode are water cooled during spraying to avoid being melted. Figure 2-13 shows a schematic of the plasma arc.

Plasma gases can be argon, nitrogen, hydrogen, helium or their mixtures. The resistance heating from the arc causes the gas to reach extreme temperatures and to form the plasma. The plasma exits the anode nozzle as a plasma plume. Then, the powder is fed into the plasma flame by using a carrier gas and an external powder port injector mounted near the anode nozzle exit. Plasma's temperature can range between 10,000-15,000°C, in this way, ceramics, metals and their composites can be melted and sprayed. The molten or semi-molten particles are accelerated towards the substrate where they will impact and form an adherent coating with the substrate. The spray distances can be in the order of 25 to 150 mm.

Particles with a size less than 5 µm cannot be carried with the plasma plume in the same way as larger particles as it would be necessary to significantly increase the carrier gas flow rate, which in turn would disturb the plasma jet and the particles' trajectory to the substrate. In addition, the fine particles do not have the mass to penetrate into the plasma plume which is very dense. Finally, powders less than 5 µm tend to agglomerate, clogging the powder feeder, carrier gas line or injector during the coating process.

A process has been developed to solve this clogging issue, which is to transport the powders with the help of a liquid carrier in which the mixture of liquid and powder forms a suspension and the process is called suspension plasma spraying (SPS) as discussed below.

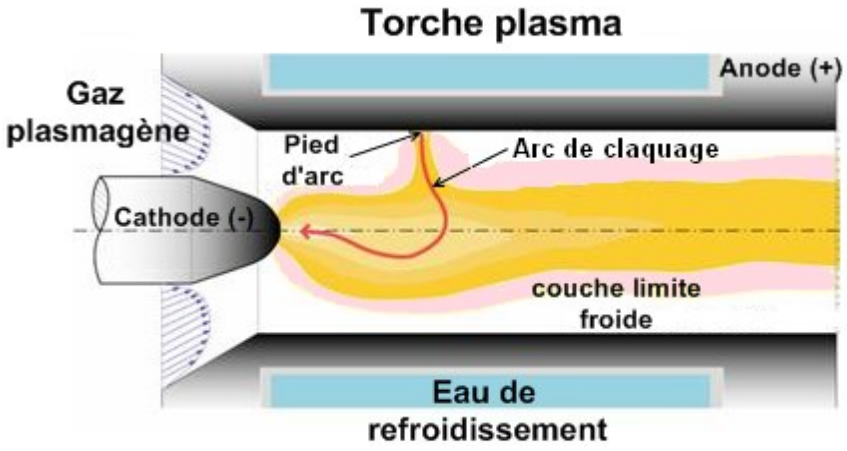

Figure 2-13. A diagram of the plasma arc and the flow of its plume. [28]

Figure 2-14. Plasma gun 3MB. [37]

2.5.2 Suspension Plasma Spray (SPS)

SPS is one of the technologies that allows one to deposit very small particles that range from 30 nm to several μm and which can produce very thin coatings [29]. In order to enhance the properties of components exposed to severe environments, stable process conditions are required in order to have high efficiency, high physical properties and repeatable deposition. SPS has been introduced recently in production for coat turbine, jet engine parts and other industrial components.

With this process, illustrated in Figure 2-15, different types of powders can be used depending on the application as shown in Table 2-1. Furthermore, the liquid used for the suspension can be; ethanol, water, a mixture of both, ethylene glycol, etc. Particles have a natural tendency to settle and stick together forming larger clusters or agglomerates hence the powder and liquid are mixed and sonicated during the suspension preparation, in order to break the agglomerated particles and to make the final suspension more homogeneous. A suspension controller can be used which will combine compressed air with the suspension mixture (similar to the aerosol principle) and this will help push the mixture through the pipes to the suspension distributer, which controls the feeding of the suspension into the nozzle and injection into the plasma plume. Once in the plume, the suspension will be heated and liquid will be evaporated

leaving the particles to be heated further and be accelerated and deposited on the target as in Figure 2-16.

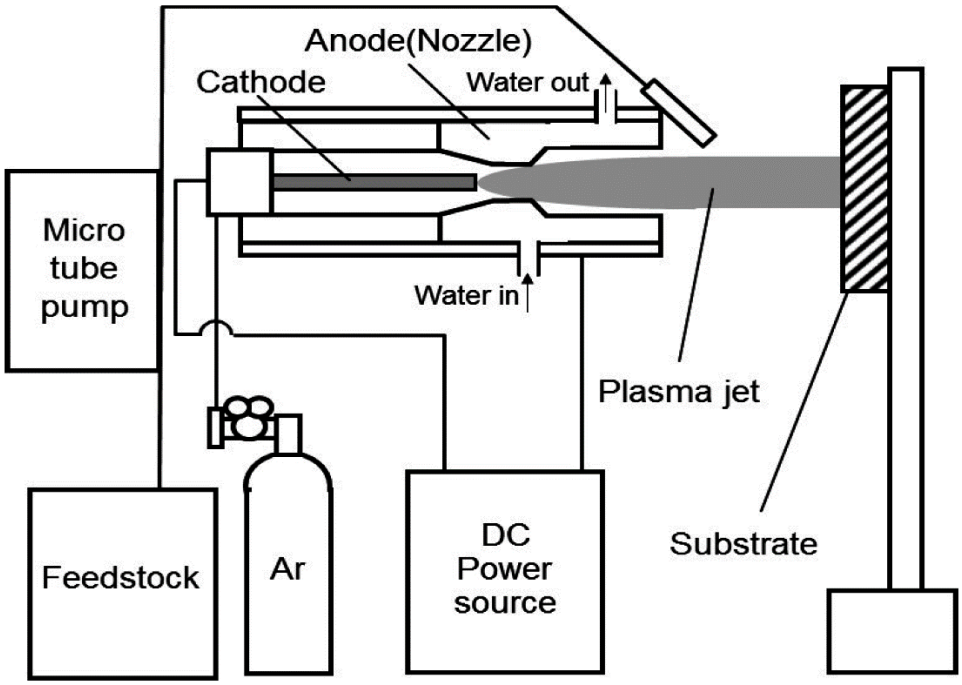

Figure 2-15. A diagram showing the Suspension feeding system used in experiments [30].

Table 2-1 Common classes of thermal spray powder materials [31].

Material Class	Typical Alloy	Characteristics	Example Application
Pure metals	zn	Corrosion protection	Bridge construction
Self-fluxing alloy	FeNiBSi	High hardness, fused Minimal porosity	Shafts, bearings
MCrAlY	NiCrAly	High temperature Corrosion resistance	Gas turbine blades
Steel	Fe 13Cr	Economical, wear resistance	Repair
Nickel-graphite	Ni 25C	Anti-fretting	Compressor inlet ducts

Oxides	Al_2O_3	Oxidation resistance, high hardness	Textile industry
Carbides	Wc 12Co	Wear resistance	Shafts

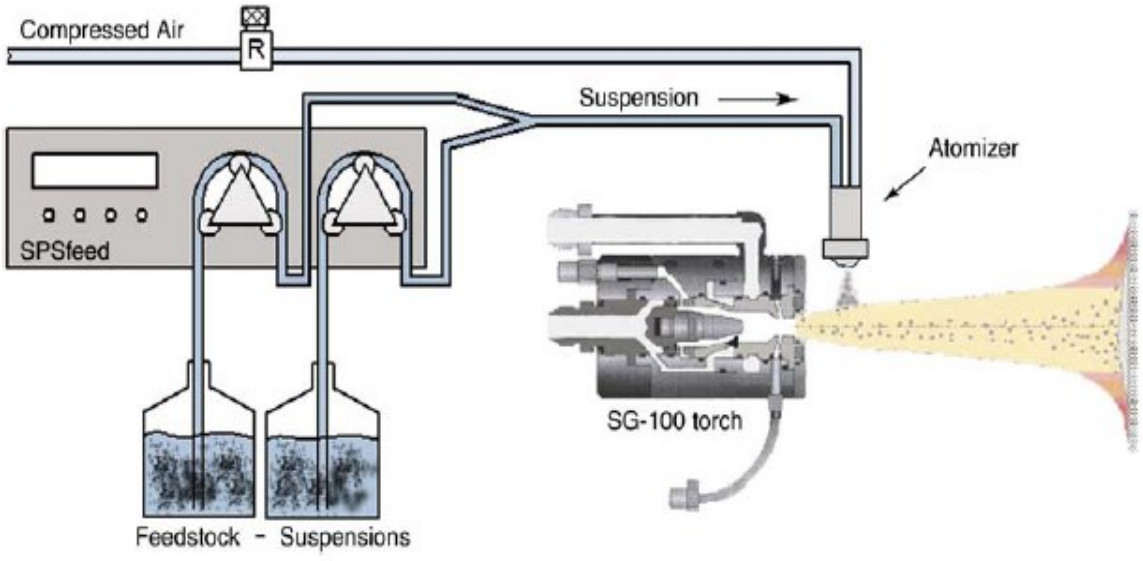

Figure 2-16. Schematic diagram of the SPS process [29].

There are 2 methods to inject the feedstock suspension into the plasma [32]:

1) Radial Injection:

This is a common method which uses a nozzle aligned almost perpendicular to the plasma plume to inject the suspension as shown in Figure 2-17 a. Note that, the suspension is usually injected as a continuous jet.

2) Axial Injection:

The suspension is injected directly through the plasma flame so less disturbance will occur to the particles. Figure 2-17 b. Note that, the suspension is atomised before it interacts with the plasma jet.

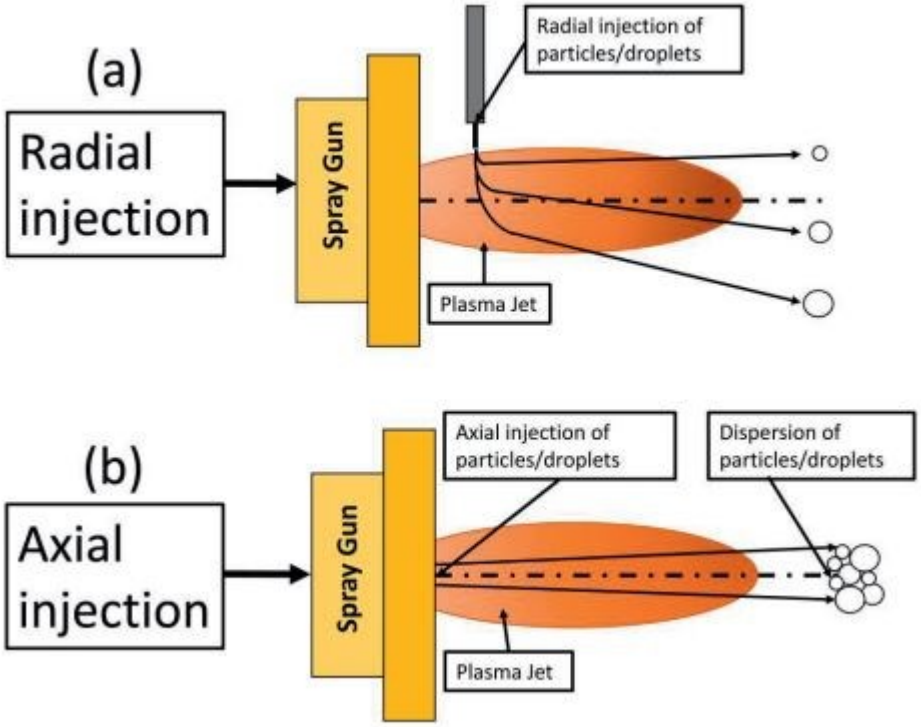

Figure 2-17. Schematics of injection mode a) Radial injection and b) Axial injection [32]

2.5.3 Thermal Spraying of Micro-textured Surfaces

2.5.3.1 Effect of SPS process parameters on coating microstructure

The type of coating and the micro-nano texture produced by SPS are dependent on a large number of process parameters, and each can affect and influence the coating in certain ways. Figure 2.18 shows a schematic of some SPS parameters. Furthermore, over 35 parameters can affect the coating, and extensive research has been dedicated to understanding the relationship between these parameters and the coating structure. A research group at Concordia University [16] was able to achieve the hierarchical texture required for superhydrophobic coatings with SCA more than 165° and SA less than 10° using a ceramic powder. Figure 2-19 shows SEM images for different types of spraying conditions and the resulting surface textures of the TiO_2 spray coatings.

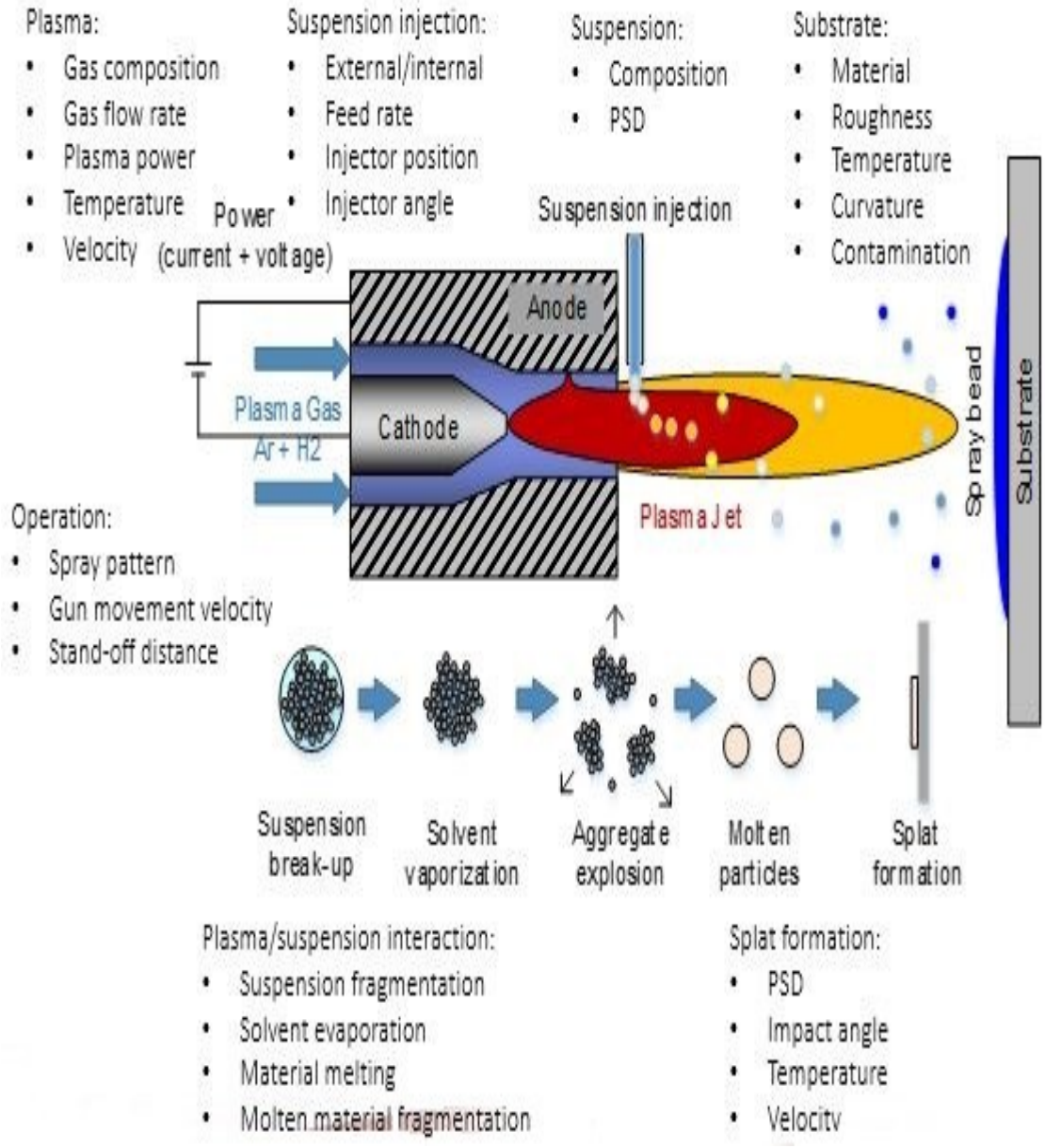

Figure 2-18. Schematic of SPS process parameters [16].

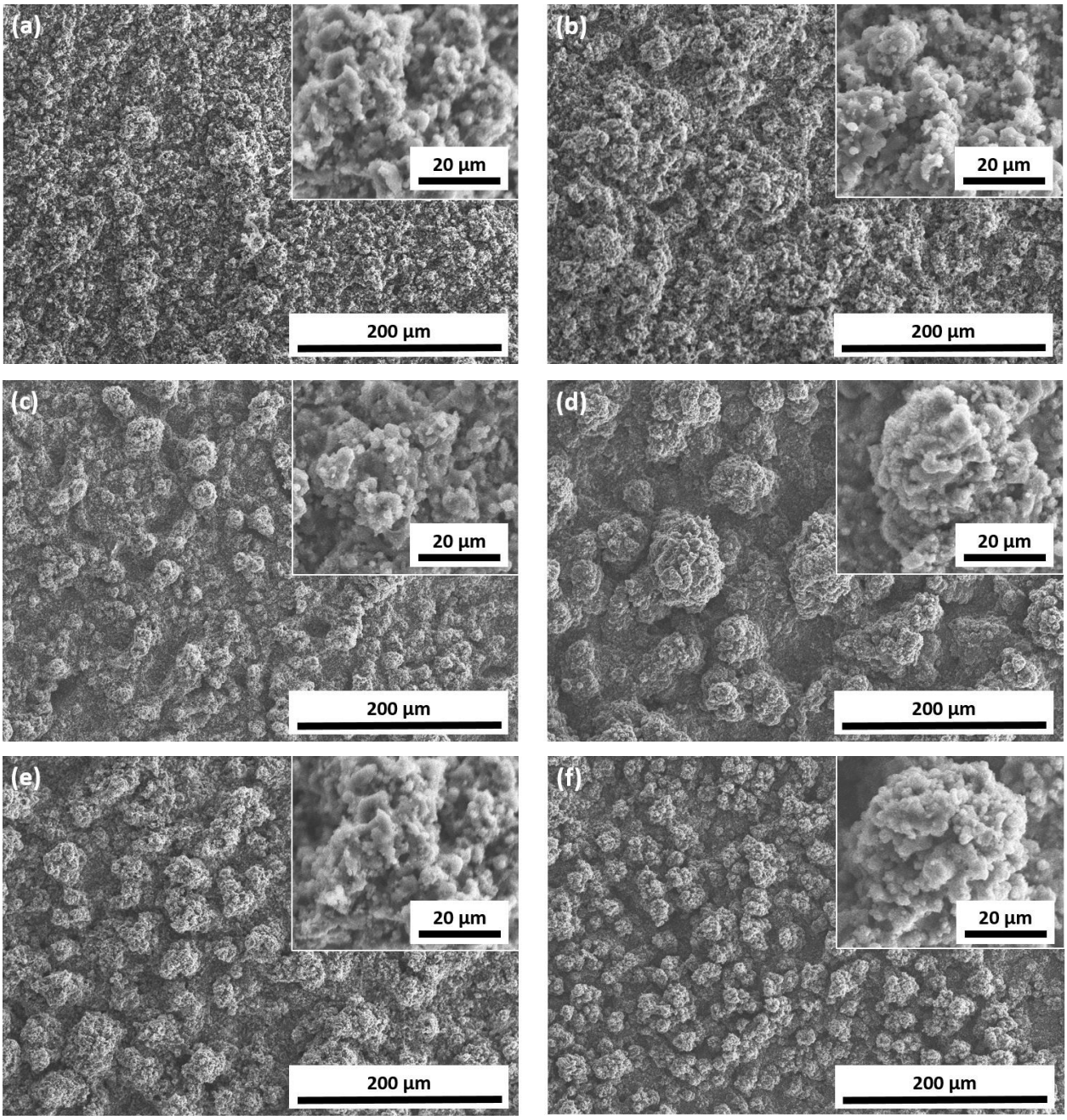

Figure 2-19. Shows SEM images of different types of spray coatings produced by varying the spraying conditions [16].

From Figure 2-19, it can be seen how the microstructure varied from fine to cauliflower-like microstructure. The mobility results, namely the *sliding angle* SA, started with a relatively high value (SA>20°) in Figure 2-19.a but decreased to SA=1.3° for the microstructure shown in Figure 2-19.f for an ethanol-based suspension of TiO_2 at high plasma power. All coatings were tested after applying a thin stearic acid layer on their surface [16].

To conclude, it is clear that a surface can change from hydrophilic or hydrophobic to superhydrophobic with a very high droplet mobility by changing the spraying conditions and resulting microstructure.

2.5.3.2 Residual Stresses

In thermal spray coatings, residual stresses [33] can result from two main sources: the "Quenching effect" when the impacting splats hit the substrate and are cooled to the substrate temperature and the stresses that arise due to the differences in thermal expansion coefficients of the splats and substrate during cooling from the deposition temperature to room temperature.

When a molten particle (1500°C) hits the steel substrate (200°C) it will contract which will lead to a high tension in the splat. The thermal expansion coefficients (α_i) of the substrate and the coated material will determine the magnitude of the residual stress: with ceramic coatings a compressive stress can occur which will cause the ceramic layer to "pop up". Note that, for a substrate with higher α_i, it can put the coating into compression and, for a substrate with low α_i, it will put the coating into a state of tension.

2.5.3.3 Durability of the Coated Material

Most of the superhydrophobic or icephobic coatings can withstand certain test regimes but not all of them (for example, ice adhesion, sand adhesion, air flow, etc.). That is why developing a surface with good durability [8] that will last a longer time with high mechanical and functional properties is the goal of many research efforts in this field.

One of the materials that has shown a promising result in the super-hydrophobicity field due to its hierarchical surface texture is TiO_2 powder. For the SPS coatings, a sub-micron sized titanium dioxide powder with an average nominal particle size of 500 nm was used in ethanol based suspension. This TiO_2 coating has been shown to have a good mechanical durability especially compared to polymer-based coatings [19].

Chapter 3. Experimental Procedure

This chapter describes the experimental procedure followed in this research work. All the spray parameters and the oil impregnation process are explained and clarified in the following sections.

3.1 Substrate preparation

All substrates were made from a flat stainless steel 304 sheet with the dimensions of 90 × 12 × 3 mm as shown in Figure 3-1 a). Before applying the coating, a grit blasting process was performed using fine alumina particles (180 grit size) with pressurized air at 350 kPa which produced a surface roughness between 1.5-2 µm, after which the substrates were cleaned with isopropyl alcohol and acetone then dried with compressed air. Subsequently, the samples were fixed to the sample holder as shown in Figure 3.1.b. Once the samples were placed on the sample holder, the latter was fixed to the table inside the spray booth, ready to be sprayed.

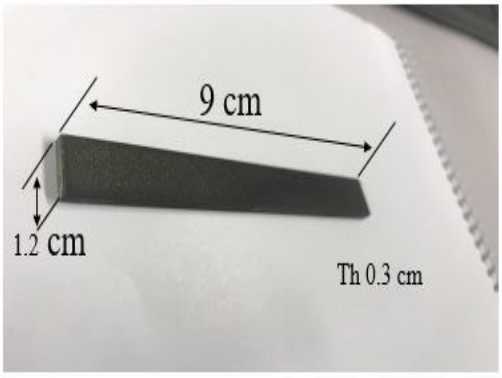

Figure 3-1. a) The substrate.

b) The substrate holder.

3.2 Suspension preparation

Creating the coating with a hierarchical texture has been done using the SPS technique. All samples were coated with a commercial submicron-sized titanium dioxide powder with average particle size diameter of 500 nm (KS-203A/B, TKB Trading, US). The rationale for using TiO_2 powder is due to its thermal/chemical stability, non-toxicity, abundance, commercial availability, low cost and good flowability. The suspension preparation started by pouring the ethanol into a glass container and then the polyvinylpyrrolidone (PVP, Alfa Aesar, US) was gradually added (5 wt% of the solid content) as a dispersant to prevent particle agglomeration and ensure the stability of the suspension during spraying. The mixing process was done by stirring with a magnetic stirrer and sonication (ultra-sound probe) with a power of 50 W during the preparation phase. After having a homogeneous mix of ethanol and PVP, ethylene glycol (E178-4) was added in order to increase the stability of the suspension. Finally, titania suspension with a concentration of 10 wt% was prepared by slowly adding TiO2 powder (1 g/min) to prevent agglomeration. Once mixed, as shown in Figure 3-2, the suspension was poured into the reservoir of the injection system. The injection system consists of two sealed pressurized tanks. The first contains the suspension and the second contains water. When a compressed gas is introduced into the tanks, it injects the suspension through the hose, up to the injector all the way into the plasma plume as shown in Figure 3-3.

Figure 3-2. The suspension.

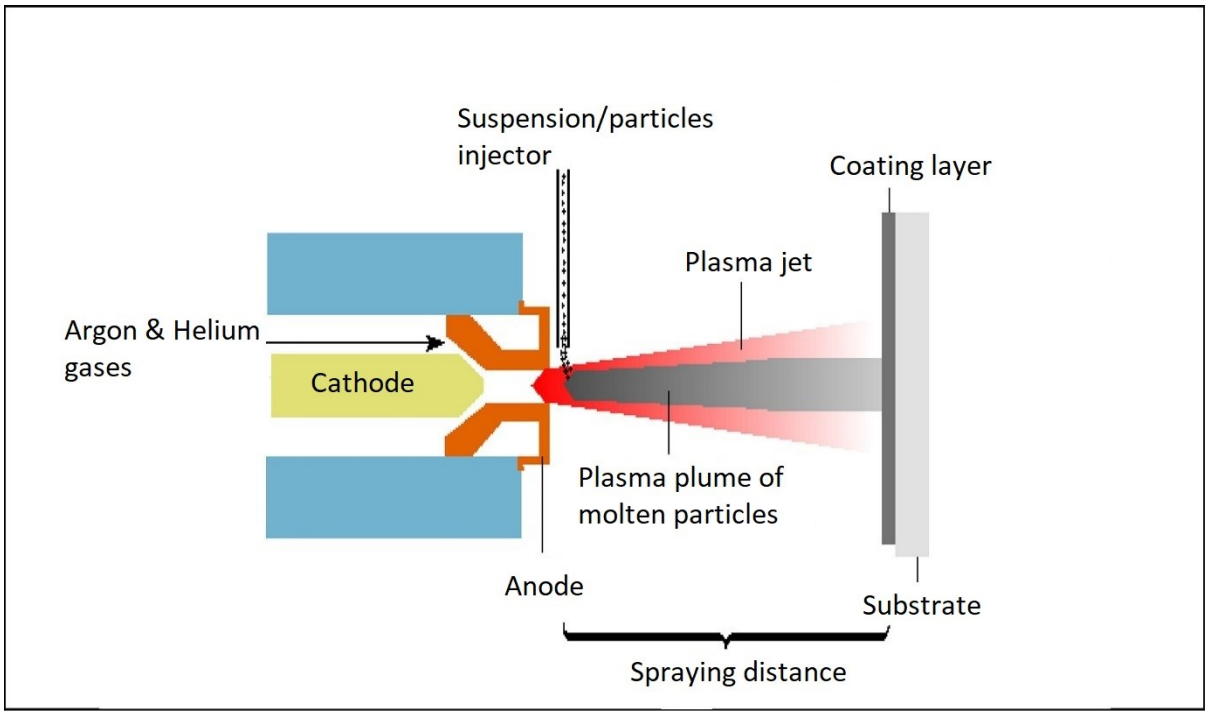

Figure 3-3. The plasma gun and the particle injector.

The particle size distribution of the suspensions was determined by a Spraytec (Malvern Instruments, UK) unit equipped with a wet dispersion accessory. The particle measurement result was D_{50} = 8 µm. The measured particle size distribution is shown in Figure 3-4 [16].

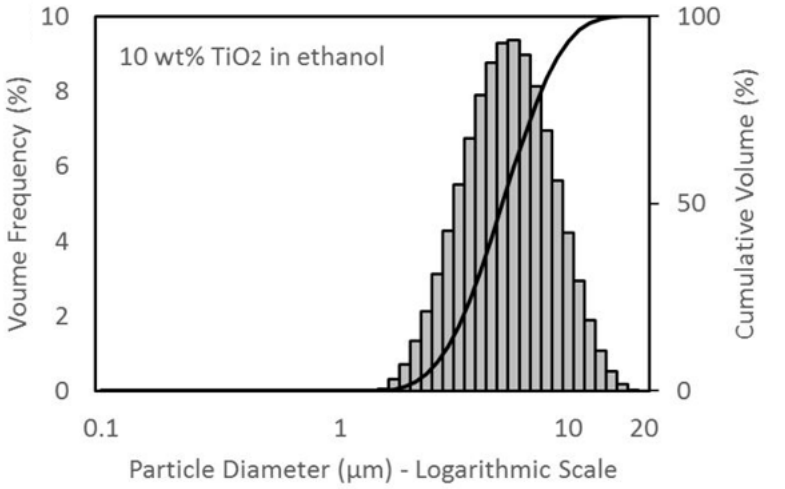

Figure 3-4. The particle size distribution of the suspension. [16]

3.3 Spray process

The process parameters can be seen in Table 3-1. The plasma gun used to deposit the coatings is a 3MB plasma torch (Metco Oerlikon, Westbury, NY). The primary gas is argon (Ar) and the secondary gas is helium (He).

Table 3-1 Spraying Parameters:

Total gas flow rate (Ar+He)	60 SLM
Voltage	50 V
Stand-off distance	5 cm
current	600 A
Feed rate	33 g/min
Power	24 kW

The spraying process includes producing several batches of coated substrates. Each batch was produced with a certain number of passes of the plasma gun in front of the substrates in order to achieve the targeted coating thickness. The goal here was to create a hierarchical texture with a certain height of micro-pillars that will act as an oil reservoir and hold the oil in place.

3.4 Coating batches

Developing micro-pillars was a key parameter for this research. The first batch of substrates included 10 passes of the plasma gun on the substrate's surface and comprises micro-pillars of heights varying between 15-25 µm. Furthermore, batches were produced with different numbers of passes; 10, 23, 50, 75 and 100 passes. Note that, each batch comprised 4 stainless steel substrates. Coating thickness produced as a function of the number of passes of the plasma gun and the arithmetical mean height of the surface (S_a) were measured by a confocal laser microscope (LEX OLS4000, Olympus, Japan).

3.5 Oil Impregnation

Before applying the oil onto the coated surfaces, a cleaning process in distilled water was performed using an ultrasonic probe for 10 minutes with 50 W of power followed by boiling in distilled water for 15 minutes. The samples were then rinsed using acetone or isopropyl alcohol and finally dried with compressed air. Oil impregnation was carried out on these cleaned hydrophilic surfaces as described below. In addition, some coatings were coated with a thin stearic acid layer by dipping them in a stearic acid solution (99.5 g 1-propanol with 0.5 g of stearic acid) and allowing the surface to dry. The thin layer, due to its low surface energy, transformed the coating hydrophilic surface to a superhydrophobic surface.

Oil impregnation was carried out by submerging the samples in oil poured in a glass container, sealing the container and then applying a vacuum of 0.12 bar for 10 minutes above the oil. Applying the vacuum removed the air bubbles which were replaced by the oil and would hopefully allow the oil to penetrate into the micro pockets as shown in Figure 3-5. Four types of lubricating oils with differing viscosities were used: 6, 125, 250 and 800 centi-Stoke (cSt).

Table 3-2 shows the properties of the oils:

Commercial Name	Viscosity @ 20°C (cSt)	Oil Density (g/ml)
Krytox KS 1220	6	-
Silicon oil	125	0.96 @ 25 °C
Krytox 143 AB	250	1.93 @ 0 °C 1.75 @ 100 °C
Krytox 143 AC	800	1.95 @ 0 °C 1.77 @ 100 °C

The rationale behind this is to find which oil provides better mobility and durability after impregnation in the ceramic coating. The next step was removing the samples from the container and allowing excess oil to drain off the coating by tilting at an angle of around 45°.

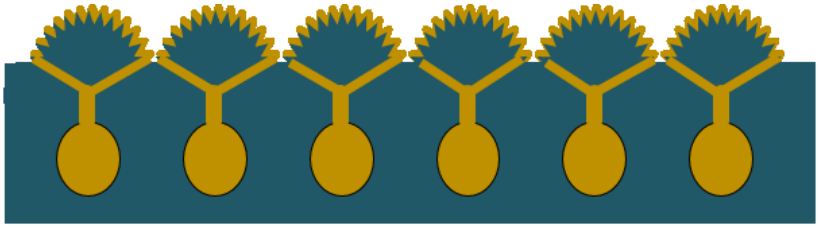

Figure 3-5. Schematic of the oil reservoir and the micro pillars.

3.6 Icing Tests

Since the goal of this study is to investigate water mobility on the oil-infused surface, wetting measurements were made before and after the icing/deicing treatments in the icing wind tunnel. In order to simulate an environment closer to reality, icing/deicing tests were carried out in Concordia's icing wind tunnel shown in Figure 3-6 a and b. The test procedure involves doing the initial water mobility measurements for reference, then fixing the sample in a substrate holder facing the flow of the air/water droplet mixture. This mixture is cooled in the closed loop wind tunnel to low temperatures to promote the formation of an ice layer on the substrate's surface. Ice formation is limited to 1 minute only since further time will only result in more ice being deposited on the first ice layer already formed. Then the water droplet jet is stopped and the samples are removed. The ice will melt at room temperature and compressed air at low pressure is used to remove the water from the surface. This icing and melting test is repeated 5 times followed by re-measuring the water mobility. If the results are promising (water mobility values are still good) another 5 cycles of icing/deicing are performed. If the mobility has been sufficiently degraded the substrate will be removed. Table 3-3 represent the test parameters in the icing wind tunnel.

Table 3-3 Icing Wind Tunnel Parameters:

Temperature	(°C)	-10±1
Air Speed	(m/s)	42
Liquid Water Content	(g/m³)	0.5
Droplet Size	(µm)	20-30
Testing Time	(minute)	1

Total number of cycles	10

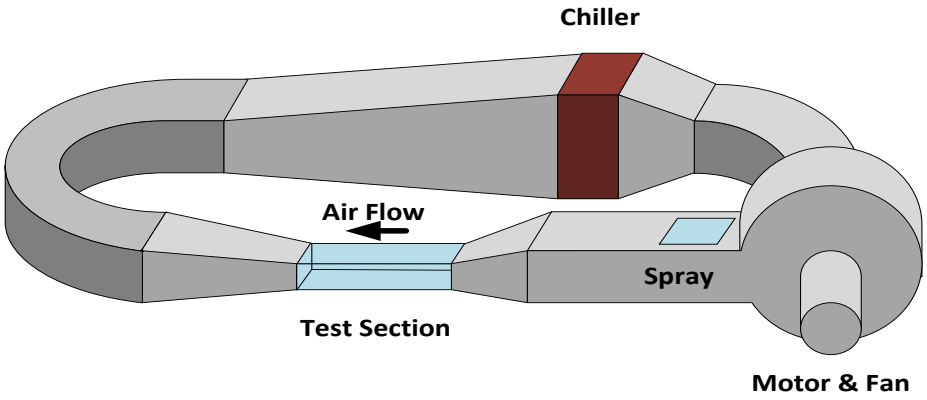

(a)

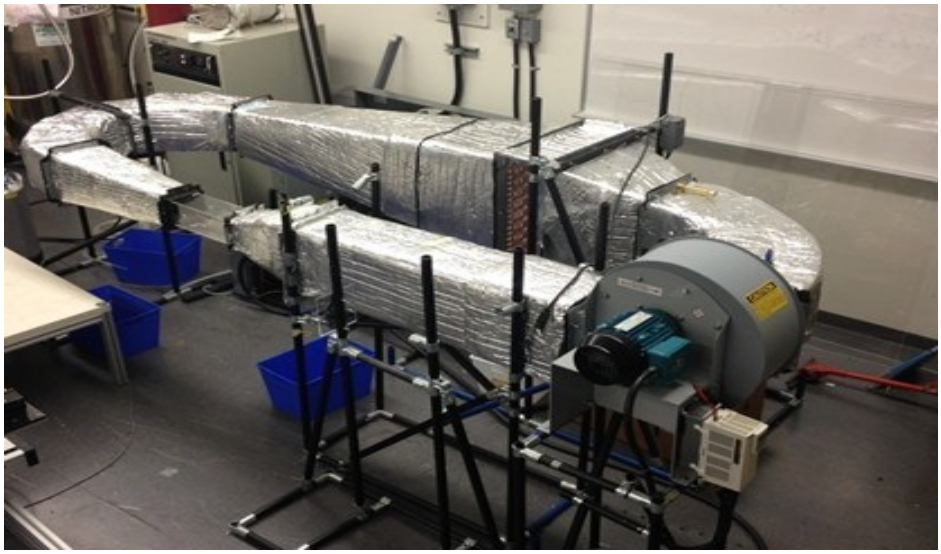

(b)

Figure 3-6. Shows the icing wind tunnel a) Schematic and b) Photograph.

3.7 Coating Characterization

3.7.1 Cross Section

After plasma spraying, samples from each batch were characterized and observed using a scanning electron microscope (SEM) (Hitachi S-3400N VP). And LEXT OLS4000 a confocal laser microscope (Olympus, Toronto, Canada). Selected samples were cut, mounted and polished in order to study their cross sections with an optical microscope. Sample sectioning was performed

with a high precision cut-off machine Secotom 15 (Struers, Canada) using a specific cutting wheel (50A15) which was selected according to the material of the samples; the cutting parameters were 3500 rpm for the cutting disk and 0.05 m/s feed rate. The cleaned samples were then mounted in a room temperature curing resin. The samples were placed in plastic molds and covered with a mixture of resin and hardener (15 ml of resin to 2 ml hardener), and were then placed inside in a vacuum chamber for 10 minutes at 0.12 bar in order to have a homogeneous impregnation and remove air pockets. After the molds were removed from the vacuum chamber they were left to cure for 24 hours. A standard polishing process was used in order prepare the surfaces for appropriate metallurgical observation at low and high magnification using MD-Plan polishing cloths with successively finer diamond pastes of 9, 3, 1 and 0.1 μm.

3.7.2 Wettability and Water Mobility

The wettability and water mobility of the prepared surfaces were studied by measuring different aspects of contact angle between water droplets and the slippery surface. Firstly, the *Static Contact Angle* (SCA) was studied by measuring the contact angle of a 10 μl droplet of distilled water deposited carefully on the slippery surface at room temperature. For each sample, 3 different droplets were photographed at different spots on the sample's surface. In order to analyze the images and measure the contact angle, an ImageJ software developed by Stalder et al. was used [35][36].

The *Sliding Angle* (SA) was measured by putting the sample on a goniometer stage and tilting the substrate to a certain angle, then depositing a droplet from a specific height and marking the angle at which the droplet started sliding on the surface.

Furthermore, the *Contact Angle Hysteresis* (CAH) was measured by slowly increasing the volume of a droplet (using a needle) on the oil-infused surface until it reaches the required volume to give the *Advancing Contact Angle* and then subsequently decreasing the droplet volume until it reaches its minimum volume to measure the *Receding Contact Angle*. This process was videoed in order to capture the droplet shape. The difference between advancing and receding contact angles was reported as the CAH. Three videos for each sample were recorded at different places on the surface and the average values were reported.

3.8 Materials and Instruments

Substrate	Stainless Steel 304 (90 × 12 × 3 mm)
Grit blasting	Fine Alumina Particles (180 grit size)
Cleaning Materials	Isopropyl Alcohol and Acetone
Powder	TiO2 with 500 nm Particle Size (KS-203A/B, TKB Trading, US)
Suspension	Ethanol based
Dispersant	Polyvinylpyrrolidone (PVP, Alfa Aesar, US) Ethylene glycol (E178-4)
Plasma Gun	3 MB plasma torch (Metco Oerlikon, Westbury, NY)
Surface modification (lowering surface energy)	99.5 g 1-propanol with 0.5 g of stearic acid
Oil impregnation Instruments:	-Vacuum machine (Citovac, Struers, Canada) -Cut-off machine (Secotom 15, Struers, Canada) -Polishing machine (Tegramine, Struers, Canada)
Oil impregnation liquids:	-Krytox KS 1220 (6 cSt, Miller–Stephenson, USA) -Krytox 143 AB (250 cSt, Miller–Stephenson, USA) -Krytox 143 AC (800 cSt, Miller–Stephenson, USA) -Silicon oil (125 cSt, Sigma-Aldrich, Canada)
Coating Characterization:	-BX53M optical microscopy (Olympus, USA) -SEM (Hitachi S-3400N VP) - LEXT OLS4000 a confocal laser microscope (Olympus, Toronto, Canada)

Finally, the self-healing test was carried out by preserving the samples within a glass container (to prevent contamination) for one week, then the droplet mobility was re-measured to see if there was any improvement in terms of low *Contact Angle Hysteresis* (CAH).

In order to reduce the healing time, after performing the icing/deicing test on some samples, heat was applied to the substrate through a hot plate for a certain time and the droplet mobility was re-measured and compared to previous data, more details concerning the heat treatment (temperature and duration) will be discussed in the result section

Chapter 4. Results and Discussion

As previously mentioned, the objective of this thesis is to investigate the development of a hierarchical microstructure, which when infused with an oil has certain water mobility properties including a low CAH and SA with good durability under harsh conditions.

4.1 Microstructure

Figures 4-1 a, b, and c show SEM images of 3 samples coated with 10, 23 and 50 passes respectively. The word "pass" represent a full scan of the plasma gun movement in front of the sample's surface. From Figure 4-1 a, it can be seen that the cauliflower-like structure is loosely distributed all over the surface, whereas in Figure 4-1 b (23 passes) the micro pillars are starting to get larger and less numerous. Finally, the cauliflower-like structures in Figure 4-1 c are fully distinguishable and the two scales of roughness on the surface are well observed. The desired hierarchical structure has been produced and the micro-clusters are well packed and distributed. There is clearly a volume between and within the micro-clusters ("cauliflowers") that can form the required oil-reservoir. Note that this structure has been produced as a result of detailed investigation and control of processing parameters e.g. the type of the grit blasting, the plasma gun stand-off distance, the plasma power, suspension solid content and plasma gas velocity [16].

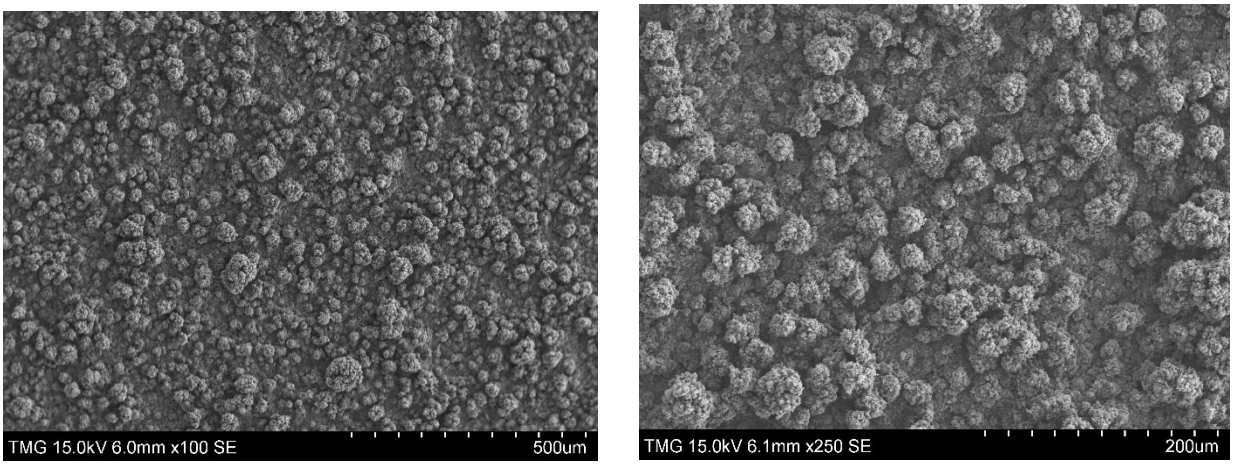

(a)

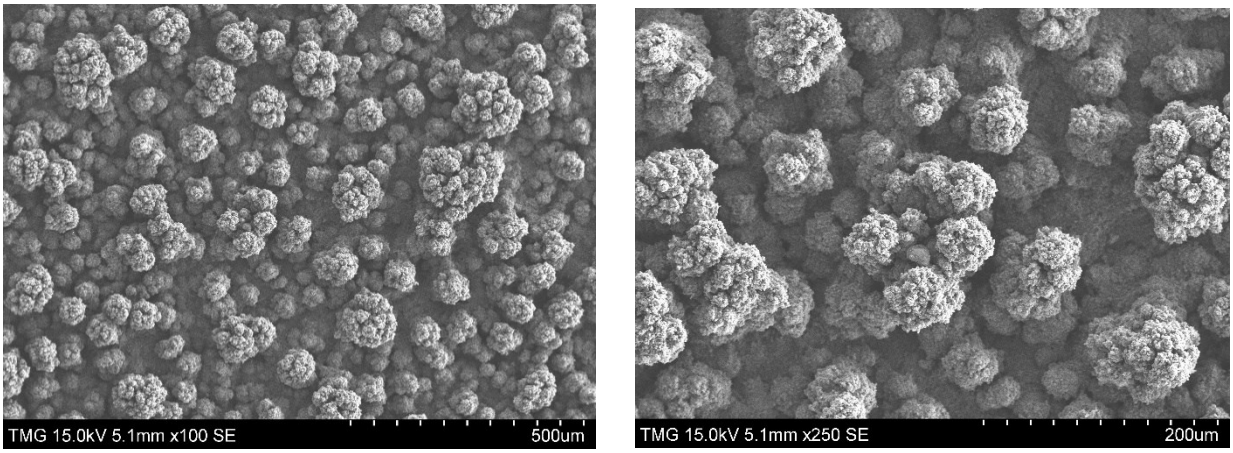

(b)

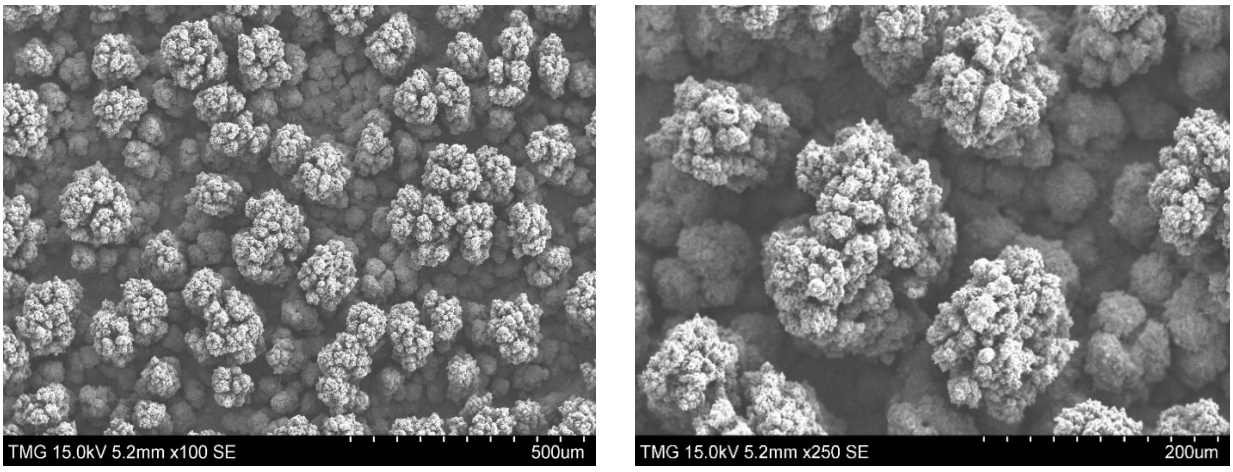

(c)

Figure 4-1. SEM images of 3 samples coated with (a) 10 passes, (b) 23 passes and (c) 50 passes.

Figure 4-2 shows the cross-sections for 2 samples coated with increasing number of passes of the plasma gun. The images shows the development and growth of the micro-pillars and the thickness of the produced coating for 50 and 75 passes which comprises pillars with heights of 160 and 275 µm, respectively.

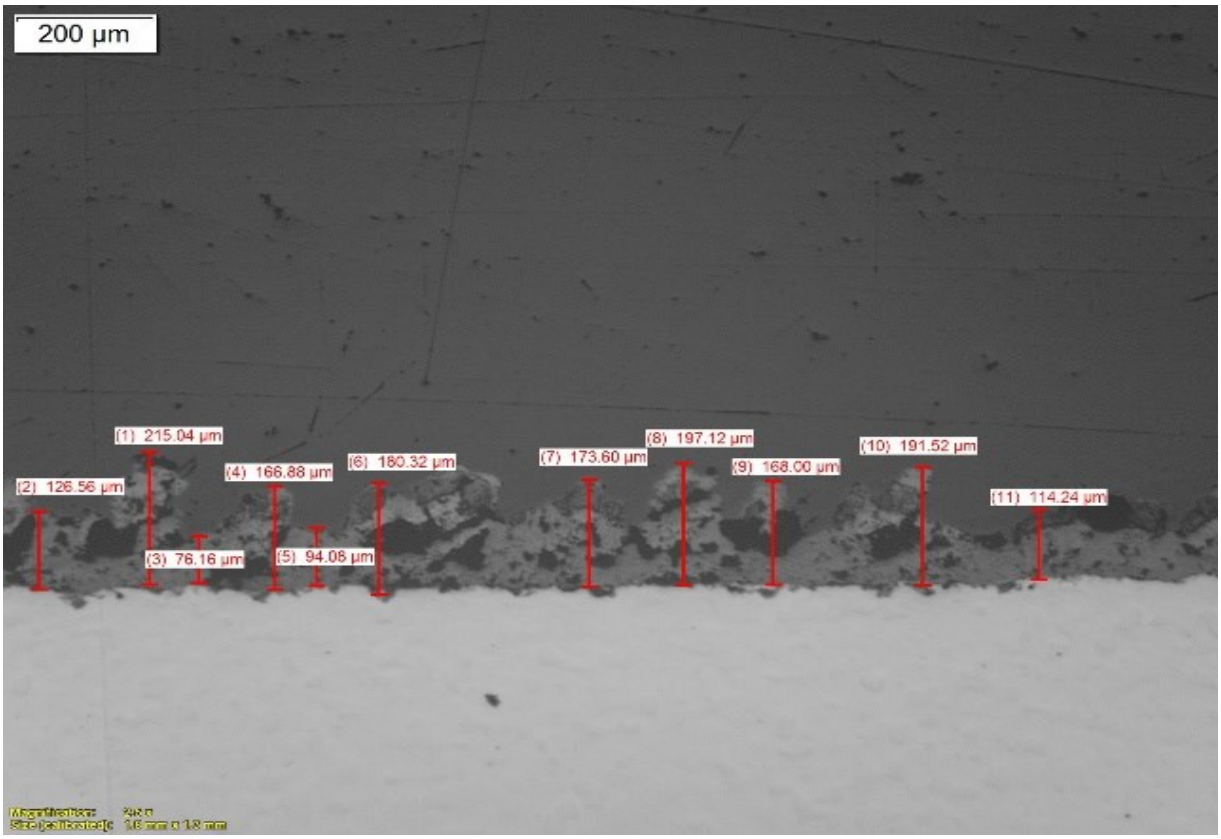

(a)

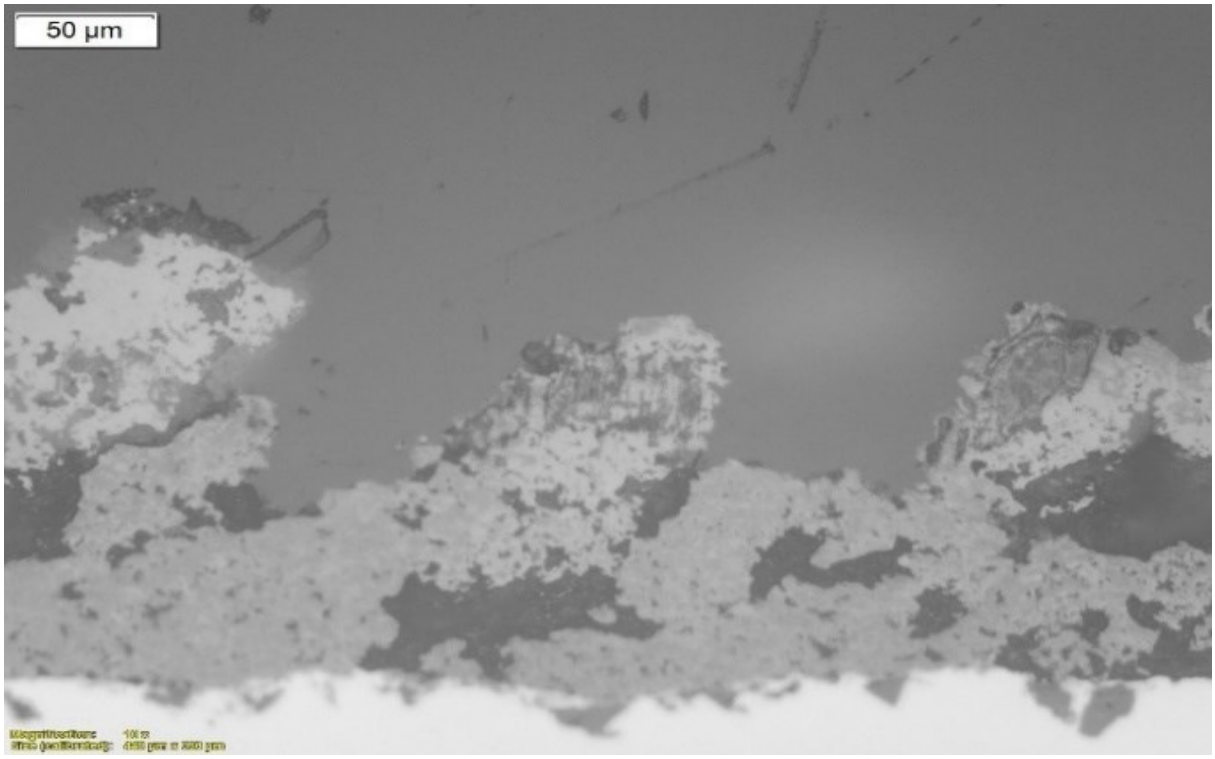
50 µm

(b)

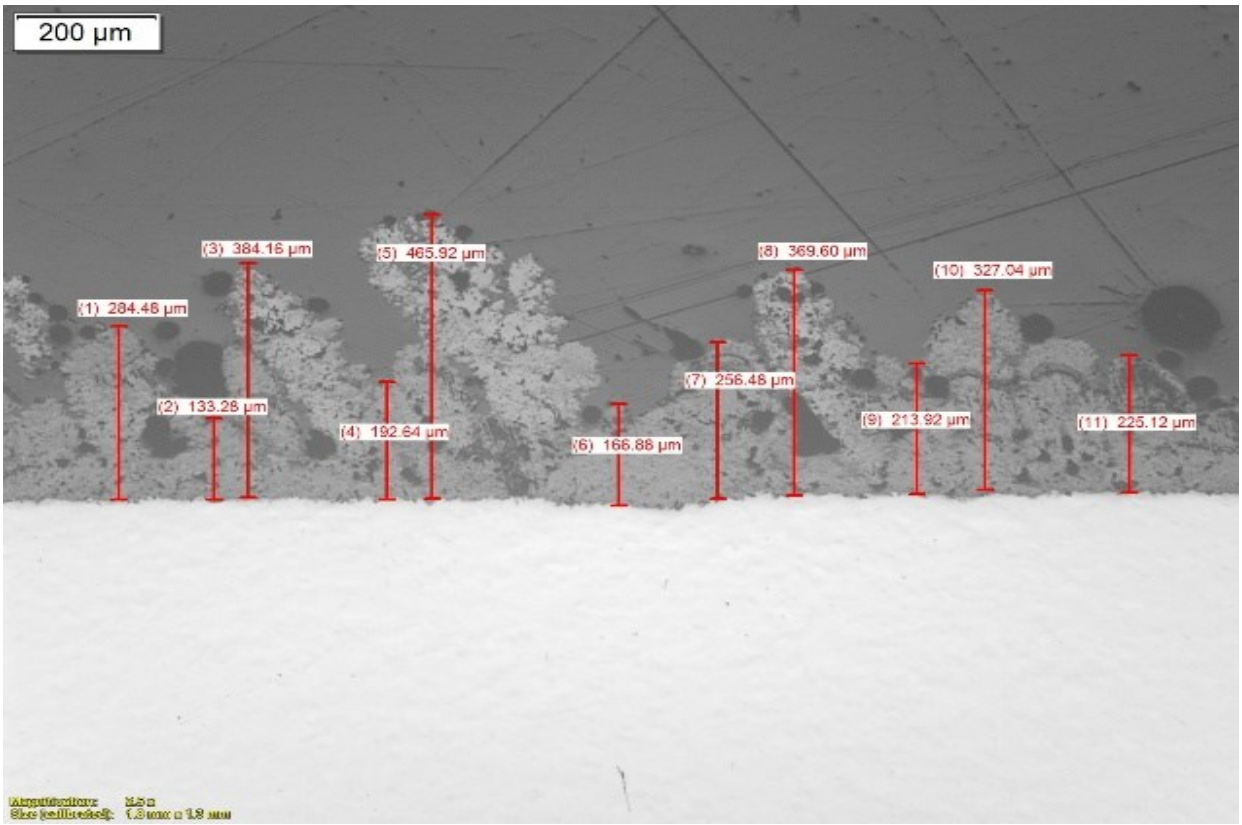
200 µm
(1) 284.46 µm
(2) 133.28 µm
(3) 384.16 µm
(4) 192.64 µm
(5) 465.92 µm
(6) 168.88 µm
(7) 256.48 µm
(8) 369.60 µm
(9) 213.92 µm
(10) 327.04 µm
(11) 225.12 µm

(c)

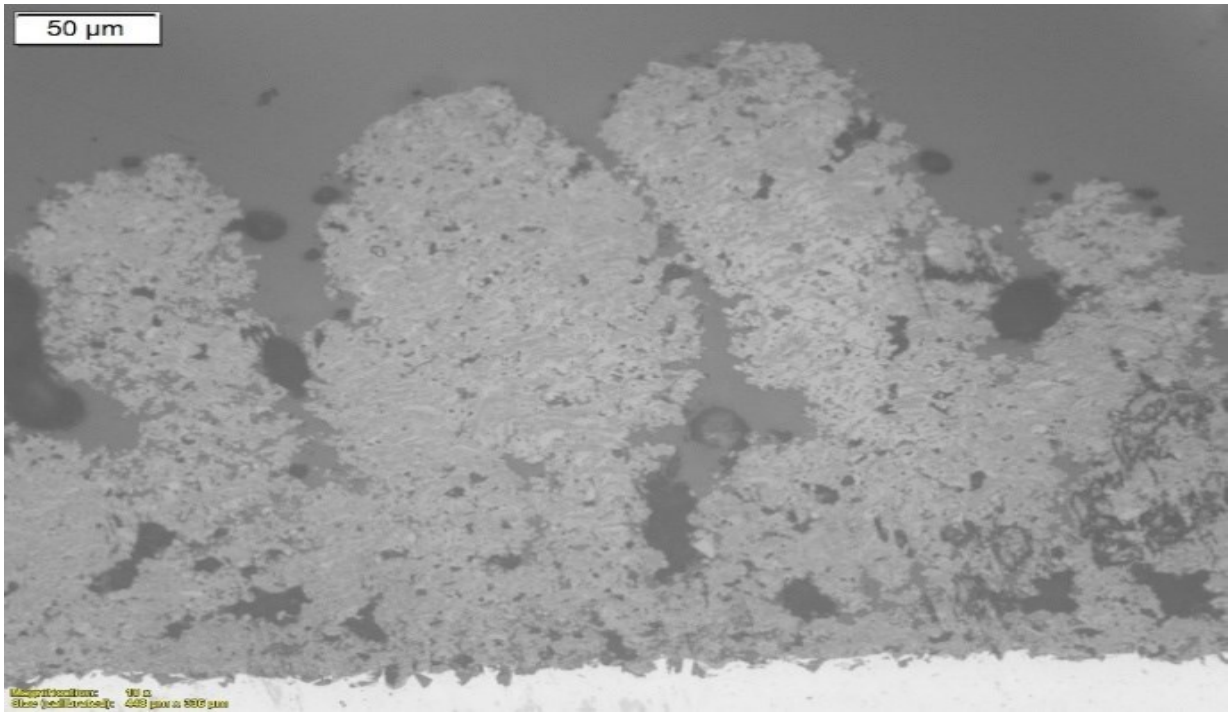

(d)

Figure 4-2. Cross-sections for TiO_2 samples after (a,b) 50 passes and (c,d) 75 passes .

Confocal laser microscopy allows one to investigate not only the surface of the sample but it gives a 3 dimensional map of the surface which can give a representation of the roughness and surface features of the coating. In Figure 4-3 (a,b) two surfaces coated with 50 passes of TiO_2 have been imaged before and after oil-infusion. The images show the difference between the coated surface with and without the oil, it's to confirm that the impregnation process has been applied successfully and that the oil filled all the gaps between the micro-pillars. Concerning the thickness of oil, it has been discussed in the upcoming paragraphs in Figure 4.10. It is not clear however if the oil is also "sucked" into the micro cavities within a particular "cauliflower".

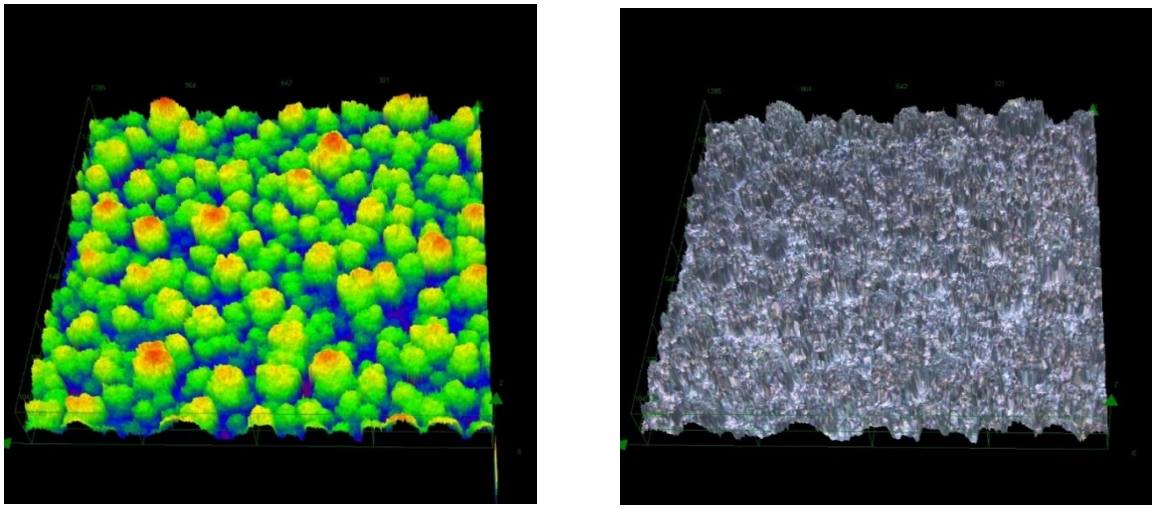

(a)

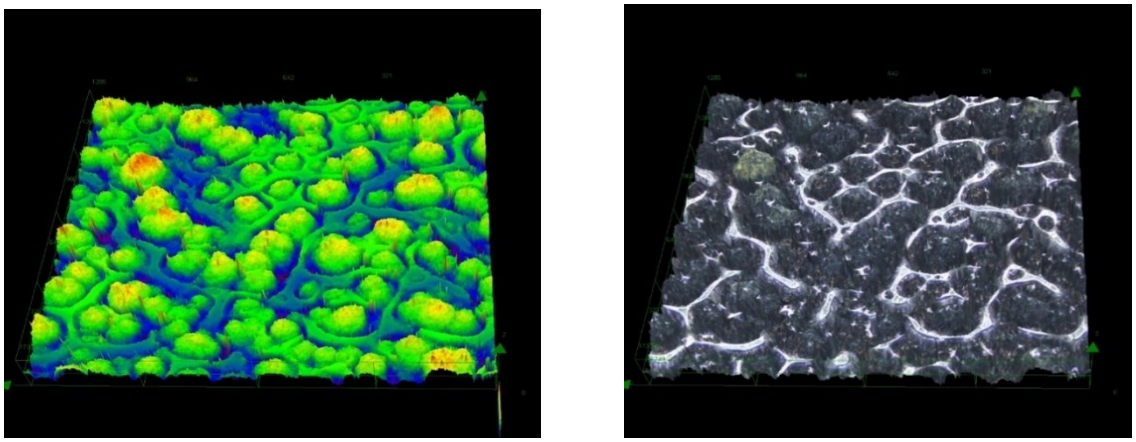

(b)

Figure 4-3. Confocal laser images of a substrate coated with 50 passes of TiO2 shows the coated surface (a) before oil impregnation and (b) after oil impregnation .

4.2 Droplet mobility of the surface

Figure 4-4 shows an example of measuring the CAH, which is the difference between the advancing (a) and receding (b) contact angles. All mobility measurements were made in a standard manner, using a 10 µl droplet of distilled water at room temperature. Figure 4-4 represents the case where the droplet is expanded and contracted on an oil-infused surface. The CAH in this case is 1.9° and as this is less than 10° the surface can be designated as “slippery”. Note that three measurements were carried out for each sample and the average of the results has been reported.

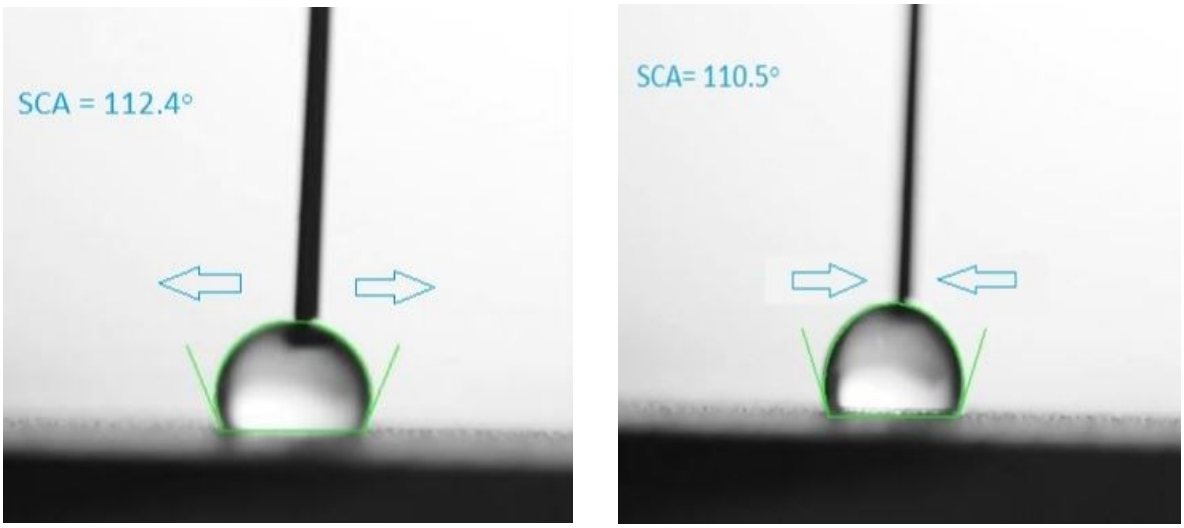

(a) (b)

Figure 4-4. Shows two images of a water droplet on an oil-infused surface when the water is (a) advancing and (b) receding. The CAH is the difference between the advancing and receding contact angles.

4.2.1 Pre-icing mobility

After plasma spraying of the TiO_2 coating on the substrate's surface, two approaches could be made for oil-impregnation: firstly, the as-sprayed coating which is hydrophilic could be infused directly with oil and the surface above the oil will be hydrophobic. Secondly, the surface could be cleaned and a post-treatment with stearic acid could be applied in order to lower the surface energy and transform it from a hydrophilic to superhydrophobic surface at which time it could be subjected to the oil impregnation process. Some researchers [12] have shown that water mobility results can be improved by transforming the surface from hydrophobic to superhydrophobic. From that point of view, the author was inspired to apply both cases and compare the results and continue the research with the method that shows the lowest CAH. Table 4-1 represent the types of the surface before oil-impregnation, non-treated, treated surface and finally after oil impregnation:

Table 4-1. Types of the surfaces:

Types of Treatment	Resulting Surface
TiO2 Coating+ Cleaning + No Oil	Hydrophilic

TiO2 Coating+ Cleaning + Oil	Hydrophobic
TiO2 Coating+ Cleaning + Stearic Acid	Superhydrophobic
TiO2 Coating+ Cleaning + Stearic Acid + Oil	Hydrophobic + very low Mobility

4.2.1.1 Water Mobility on a hydrophobic surface

Table 4-2 represents the water mobility results after oil-impregnation of the as-sprayed hydrophobic surface including SCA, CAH (mean and standard deviation) and SA. The mobility has been measured for two different thicknesses: Thin and Medium, which refer to the height of the micro-pillars, 70 and 160 µm, respectively. Four different oils with distinct viscosities were also investigated. The results were collected after 2 and 48 hours of oil-impregnation in order to see if a longer time allows more penetration of the oil into the micro-pockets.

Table 4-2. Mobility results of a hydrophobic surface:

Oil viscosity (cSt)	Infusion time (h)	Coating Thickness	SCA (°)	CAH (°)	SA (°)
6	2	Thin	125±3	NA	NA
6	48	Thin	139±5	NA	NA
6	2	Medium	122±3	NA	NA
6	48	Medium	141±4	NA	NA
125	2	Thin	71±2	5±3	11
125	48	Thin	82±3	28±5	>20
125	2	Medium	90±1	4±2	8
125	48	Medium	85±3	29±3	>20
250	2	Thin	109±3	14±5	18
250	48	Thin	112±4	16±6	>20
250	2	Medium	102±1	6±1	9

250	48	Medium	109±1	11±3	12
800	2	Thin	106±2	14±3	19
800	48	Thin	117±4	47±7	>20
800	2	Medium	107±2	18±1	12
800	48	Medium	121±2	38±3	>20

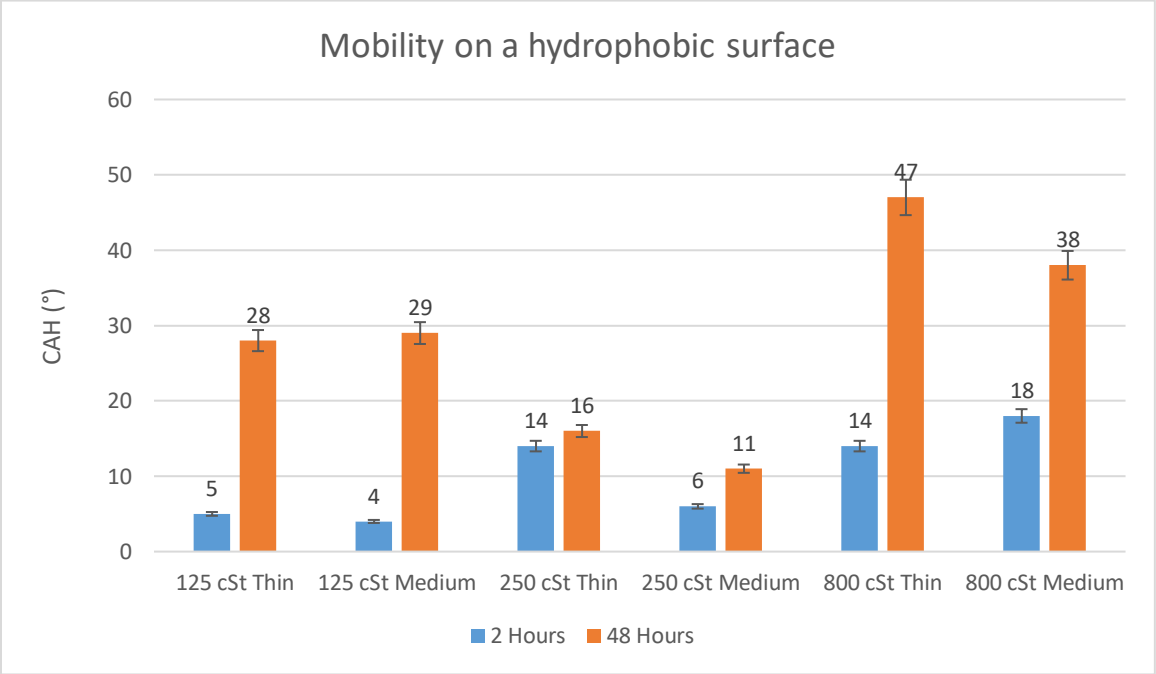

Figure 4-5 Changes in CAH of different coatings with different oil viscosities per exposure time on a hydrophobic surface.

In Table 4-2, the CAH for the low viscosity oil (6 cSt) is listed as Not Applicable (NA) because the oil with a very low viscosity did not behave well with the ceramic coating. Even with the hierarchical structure, the oil did not remain in place once the substrate was tilted. The oil drained from the surface and pores. Also the oil with high viscosity (800 cSt) had a decrease in mobility after 48 hours of impregnation. The oil did not stay on the surface: it stayed inside the micro pockets. From Figure 4-5 we can conclude that the two medium viscosity oils (125 and 250 cSt) give promising results after 2 and 48 hours. In other words, the last mentioned oils were able to remain in the micro-pockets and not drained from the surface; that is why they were selected

for further testing. To summarize, 6 and 800 cSt oils did not show low mobility results because they did not behave well with the ceramic coating, for the very low viscosity oil, it slipped from the surface and for the highest one it remained in the micro pores due to high viscosity. Back to the medium viscosity oils (125 and 250 cSt) they showed good results in terms of low mobility after 2 and 48 hours of oil impregnation, both of them were able to penetrate to the micro pores and be retrieved to the surface once again when needed. Due to that reason we continued the research with the 125 and 250 cSt oil.

4.2.1.2 Water Mobility on a superhydrophobic surface

Table 4-3 represents the data collected from 3 samples; **Thin, Medium and Thick** (70, 160 and 270 μm thick coating, respectively). A thicker coating was introduced as it was thought that by increasing the height of the micro-pillars more oil could be stored in the micro-pockets which will be easier to retrieve to the slippery surface properties over a longer period. The as-sprayed coatings were cleaned and treated as described in Section 3.5 to produce the superhydrophobic surfaces After being impregnated with one of the two oils with middle viscosity (125, 250 cSt) water mobility results were measured as previously described.

Table 4-3 Water mobility results of a superhydrophobic surface

Oil viscosity (cSt)	Infusion time (hours)	Coating Thickness	SCA (°)	CAH (°)	SA (°)
125	2	Thin	93±0.5	6±1.5	11
125	48	Thin	117±1	18±2	15
125	2	Medium	90±0.5	5±0.5	11
125	48	Medium	113±1.5	6±1.5	12
125	2	Thick	86±1	5±1.5	19
125	48	Thick	91±3	8±2	>20
250	2	Thin	107±0.5	6±1	10
250	48	Thin	95±1	7±1	12
250	2	Medium	109±0.5	4±1	8

250	48	Medium	90±3.5	5±1.5	9
250	2	Thick	103±1	11±2	19
250	48	Thick	120±3	13±4	>20

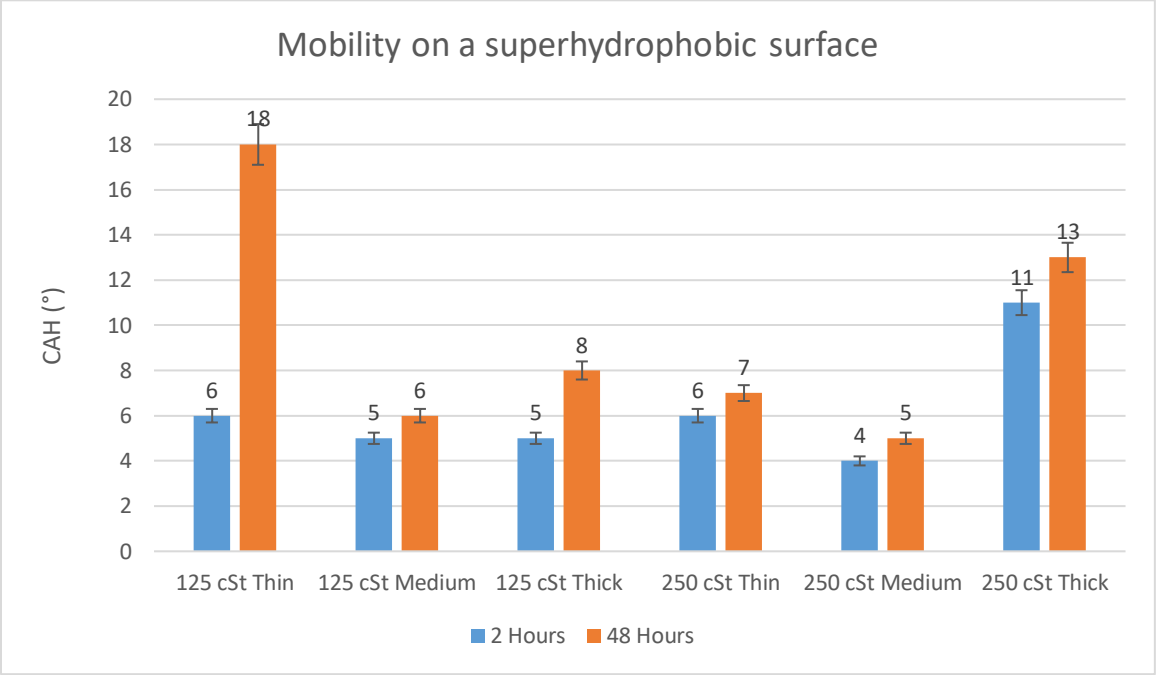

Figure 4-6 Change in CAH of different coatings with different oil viscosities per exposure time on a superhydrophobic surface.

The results in Table 4.3 show that for all cases, the CAH increases on the oil-infused samples when measured after 48 hours compared to 2 hours after impregnation. This change is most dramatic for the thin coating with the 125 cSt viscosity oil, which indicates that this combination cannot maintain a good droplet mobility. The thin coating with 70 µm thickness did not succeed in creating the required micro-pocket volume to preserve the oil. Figure 4-7 shows the gaps between the pillars. Note that, the first mobility measurements (mobility of a hydrophobic surface) were to identify which types of oils behave better with the ceramics according to certain coating thickness, while the second test of mobility measurements (mobility of of a superhydrophobic surface) were to identify which coating thickness behave better and keep the oil for 48 hours without a huge variance in the mobility results.

Furthermore, comparing the results for the CAH between hydrophobic and superhydrophobic surface, Figure 4-8 shows that the CAH values dropped to an angle of about 5° in the case of the superhydrophobic (stearic acid + oil) surfaces both at 2 and 48 hours whereas the oil-only surface showed these CAH values after 2 hours but after 48 hours the values deteriorated significantly. It can be seen that the presence of stearic acid (Superhydrophobic surface) gives consistent results in terms of low CAH compared to a (Hydrophobic surface) with a long impregnation time. In other words, creating a slippery surface with low mobility measurements can be achieved by applying the oil impregnation process on a superhydrophobic surface

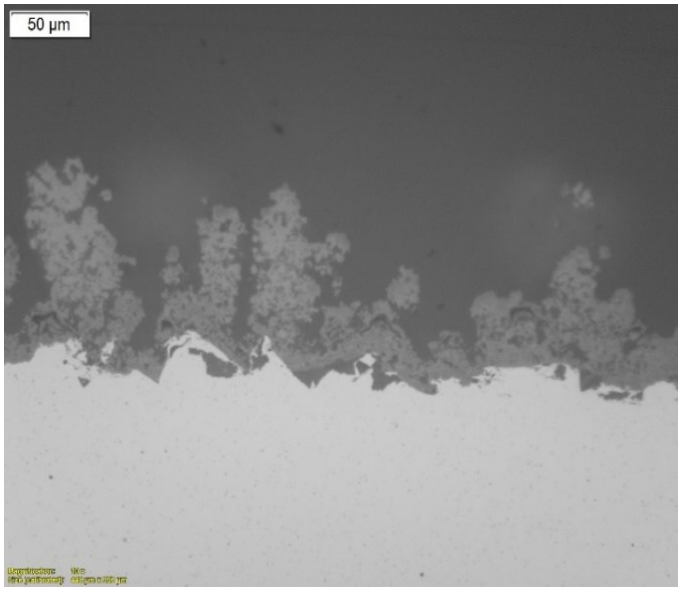

Figure 4-7 Cross section of the Thin TiO2 coating (70 µm thickness) showing the narrow gaps between the pillars.

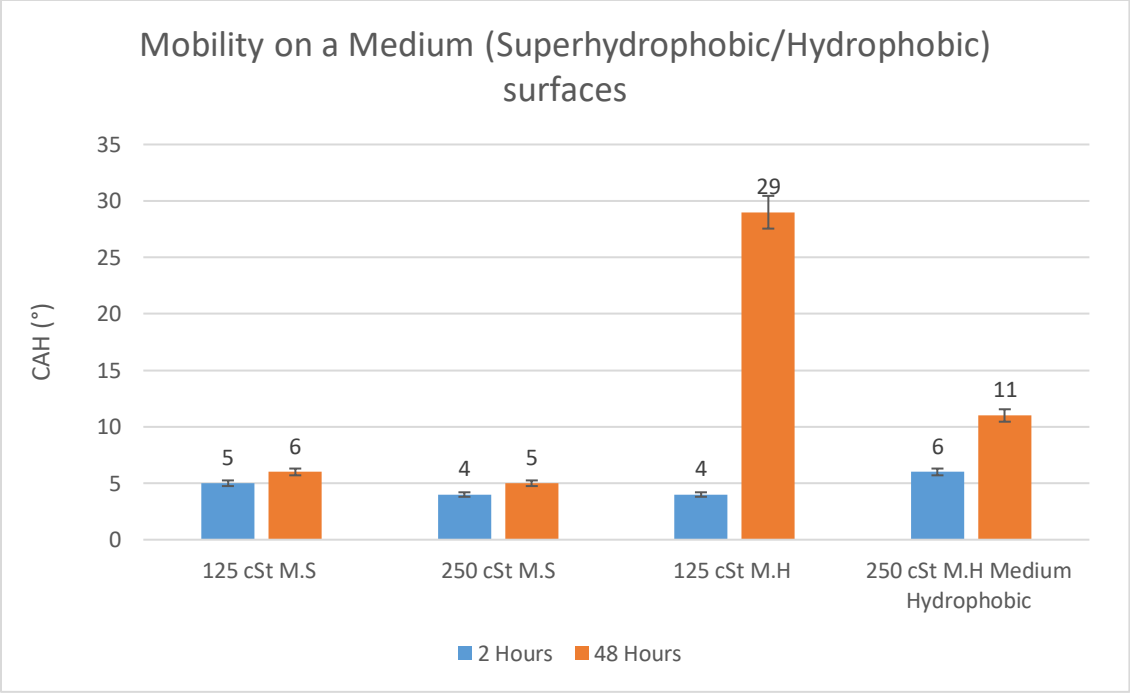

Figure 4-8 Comparison of the observed mobility on the medium coating (160 µm thick) with (Superhydrophobic) and without (Hydrophobic) stearic acid treatment after impregnation with the 125 and 250 cSt oils.

4.2.2 Icing wind tunnel tests

After reviewing the data from samples with different thicknesses it was concluded that the best combination is a coating thickness of 160 µm thickness (Medium with 50 passes) with either the 125 or 250 cSt viscosity oil as this gives good results in terms of keeping a low CAH and also of creating the needed oil-reservoir. Going forward, these combinations were used for testing in repeated icing cycles in the icing wind tunnel in order to study the behavior of the oil-infused surfaces in such conditions.

Table 4-4 and Figure 4-9 represent the data for samples with medium thickness (50 passes) tested in Concordia's Icing Wind Tunnel (IWT) at the maximum power (air velocity 43 m/s and temperature -10 ±1°C). The measurements were carried out before the icing test (reference point) and after 5 and 10 cycles of icing-deicing. Note that only 2 types of oils were used (silicone oil with 125 cSt and Krytox fluorinated oil with 250 cSt). Table 4-3 shows that before icing tests begin, both oils behave well in terms of low CAH but after 5 cycles for the silicone oil (125 cSt) infused coating, the CAH had increased significantly to more than 20°, and after 10 cycles it was 45°. On the other hand, Krytox oil (250 cSt viscosity) maintained a CAH below 10° after 5 cycles,

but after 10 cycles it had increased to 27°. Due to these findings, the Krytox oil with 250 cSt was used for the next step of experiments. The increased CAH observed after a number of icing/deicing tests (Figure 4-9) is likely due to the gradual removal of the oil at the top surface of the TiO_2 pillars in each icing/deicing test. This aspect will be further investigated in the following section.

Table 4-4 Mobility results after icing cycles:

Oil viscosity (cSt)	Time (cycles)	SCA (°)	CAH (°)	SA (°)
125	Before icing	93±3	2±0.5	8
125	5	97±3.5	24±5	>20
125	10	103±5	45±5.5	>20
250	Before icing	112±4	4±1	8
250	5	119±5	7±1.5	12
250	10	129±5.5	27±3	>20

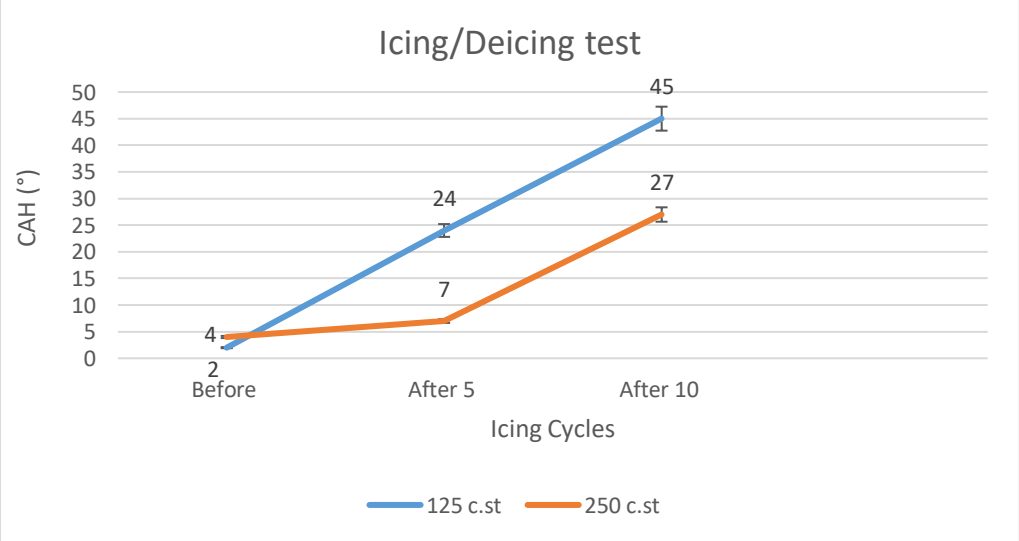

Figure 4-9 Change in CAH of different coatings with different oil viscosities per exposure time for the icing-deicing test.

To conclude, in the case of a superhydrophobic surface (treated surface) longer exposure time to icing leads to decrease of the oil's height allowing the exposure of the stearic acid layer

that remains on the micro-pillars. In other words, if the oil layer is removed, a stearic acid layer will be revealed to the surface preventing the water droplet from sticking to the surface (lower CAH). While in the case of a hydrophobic case (non stearic-treated surface) when the oil decreases it will expose the micro pillars that are already hydrophilic and the water droplet will stick to the surface, meaning the mobility will decrease (higher CAH).

4.2.3 Self-healing of the oil-infused coating

If the increasing CAH is due to the oil removal as mentioned above, it should be possible to recover low CAH if one permits the oil to recoat the pillar tops. The oil can flow back to the top of the pillars due to the capillarity force and its relatively low viscosity. This is the object of this section.

4.2.3.1 Without a heat source

After completing the icing/deicing test for 10 cycles, the samples were kept in a sealed glass container for 1 week at room temperature then the mobility test was repeated to study if there was a change in wetting behavior after a "rest" period. From the values given in Table 4-5, the contact angle hysteresis CAH dropped back to around 7° which is similar to the value after 5 cycles of icing/deicing. The reason behind this "self-healing feature" is presumed to be the action of capillary forces that succeed in redistributing oil from between or within the micro-pillars to the surface regions and thus reduce the CAH values and improve the water mobility.

Table 4-5 Water mobility results presenting the self-healing feature:

Time	Thickness (µm)	SCA (°)	CAH (°)	SA (°)
Before icing	160	112±4	4±1	12
After 5 cycles	160	119±5	7±1.5	8
After 10 cycles	160	129±5.5	27±3	>20

1 week	160	121±6	7±3.8	18

4.2.3.2 With a heat source

In an attempt to reduce the healing time from 1 week or more, the impregnated sample was heated for a short time. Thus, after the oil impregnation process was performed on a sample with a superhydrophobic surface followed by 10 cycles of icing/deicing, the sample was exposed to a heat source using a hot plate for 10 minutes at 100±5°C. The results can be seen in Table 4-6. The table shows that the static contact angle has increased to152° which is significantly higher than it was before the icing test (103°), this increasing is probably due to accelerating the chemical reaction between the oil, stearic acid and air interfaces. The CAH has decreased back to approximately the same value as after the first 5 icing cycles. After heating the sample, it appears that it is possible to redistribute the oil from in-between the micro pillars to the surface by lowering the oil's viscosity without burning the oil. The Krytox oil (143 AB) can withstand a temperature range of -40 to 232 ºC without significant degradation.

Table 4-6 Mobility results after heating the iced/de-iced oil-infused surface.

Time	Thickness Type	SCA	CAH	SA
Before Icing	Medium	103±2	3±1	13
After 5 cycles	Medium	116±2	12.5±1	>20
After 10 cycles	Medium	126±3	21.7±3	>20
Heating	Medium	152±3	13.6±3	19

The following images from the confocal laser microscope show the changes in surface composition/appearance of the samples before (Figure. 4-10 a) and after oil impregnation (Figure. 4-10 b) and also after the icing cycles (Figure. 4-10 c) and finally after the heating process (Figure. 4-10 d).

Figure 4-10 a shows the hierarchical structure, in other words, the base coating layer and the micro pillars without any oil can be observed, moving on to Figure 4-10 b it shows the sample after impregnating it with the Krytox (250 cSt.) oil for 10 minutes. The oil is clearly visible on the surface as large rivulets and smaller half-rings (C-shapes). Furthermore, Figure 4-10 c shows the sample after 10 icing/deicing cycles in the IWT at the maximum power (air velocity= 42 m/sec) at -10±1°C. It is apparent from the Figure 4-10 c that much of the oil at the surface has been removed. It is unclear how much oil still remains. The image after icing/deicing in Figure 4-10 c are very similar to the images before oil-infusion. However, the wetting results after the "healing" treatment and the images in Figure 4-10 d clearly indicate that oil has been brought back to the surface. This oil must have been at the bottom of the micro-pillar pockets or inside the porous "cauliflower" structures, or both places, after the icing/deicing cycles in order for it to have been brought back to the surface during the healing treatment. Note that, Figure 4-10 d represents the substrate surface after heating it at 100°C±5°C for 10 minutes and it can be seen that some oil is returning to the surface. In other words, heating the substrate and oil has increased the speed of the "self-healing" process and the "healing" time has been reduced from 1 week at 25°C to 10 minutes at 100°C.

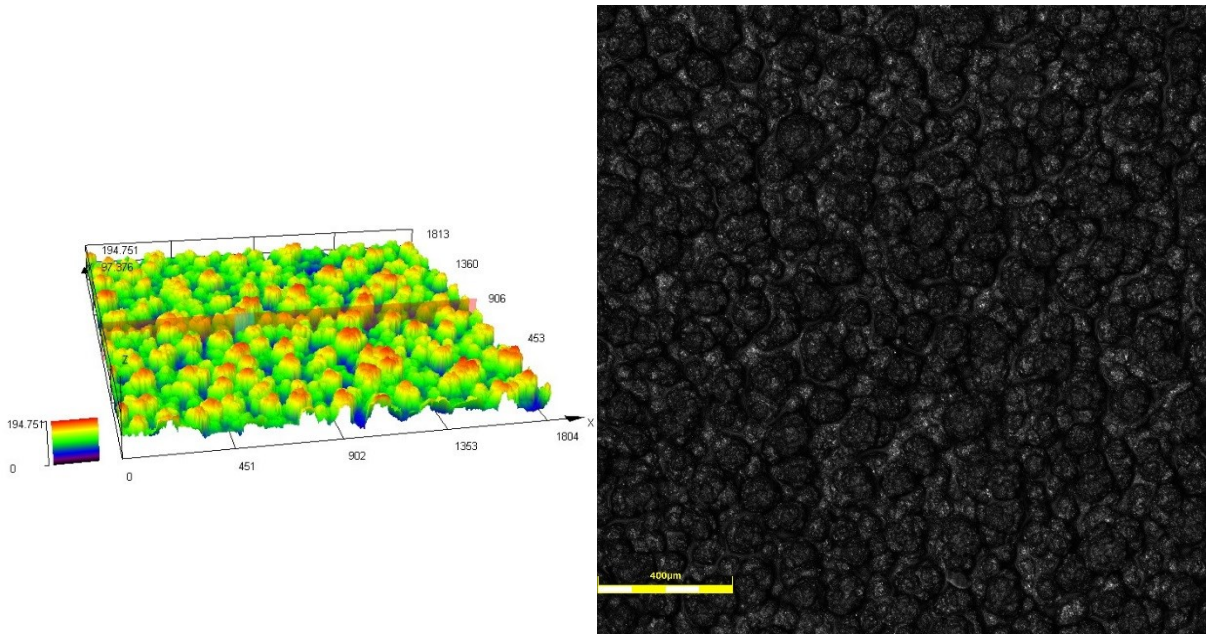

(a)

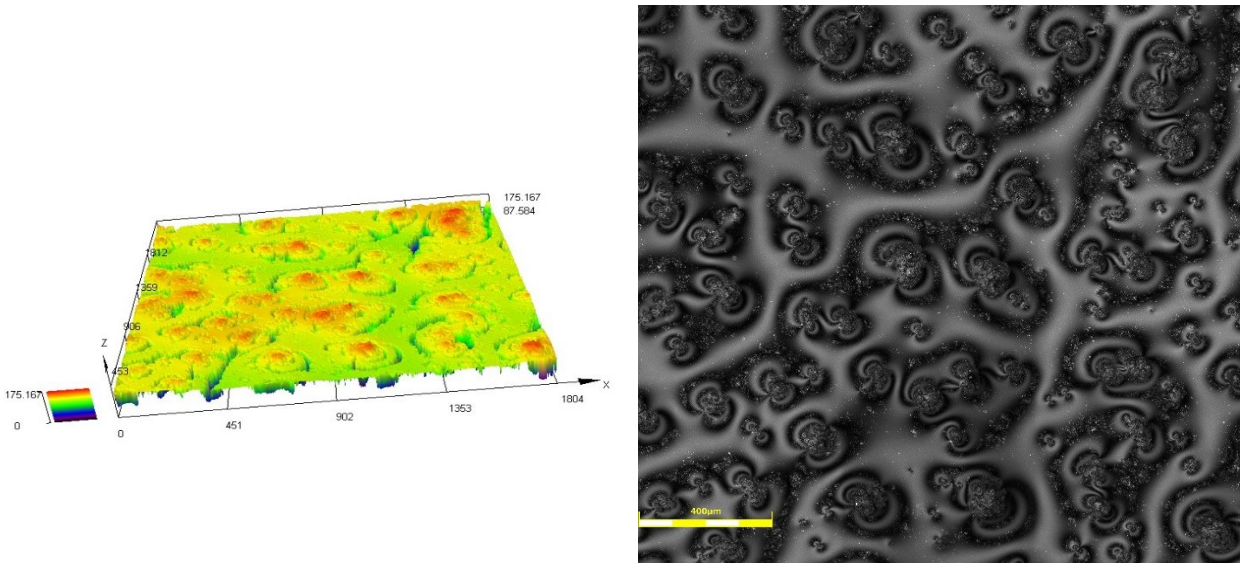
175.167
87.584
1812
1359
906
453
Z
X
175.167
0
0
451
902
1353
1804
400µm

(b)

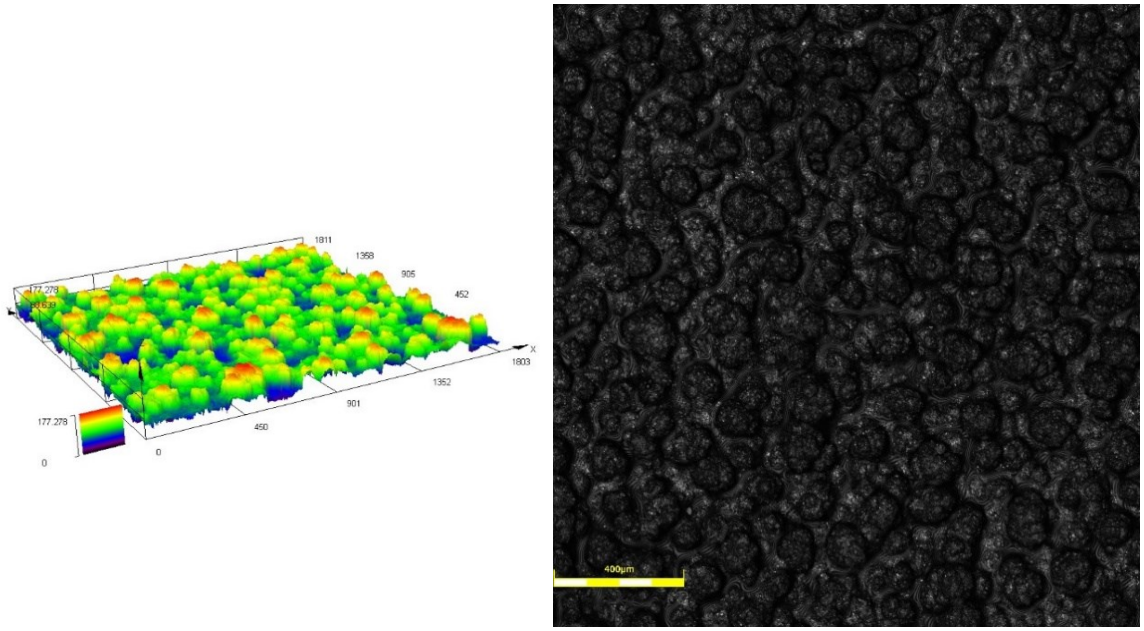
1811
1358
905
452
177.278
X
1803
1352
901
450
177.278
0
0
400µm

(c)

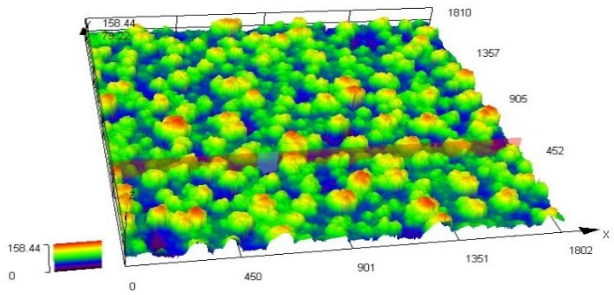

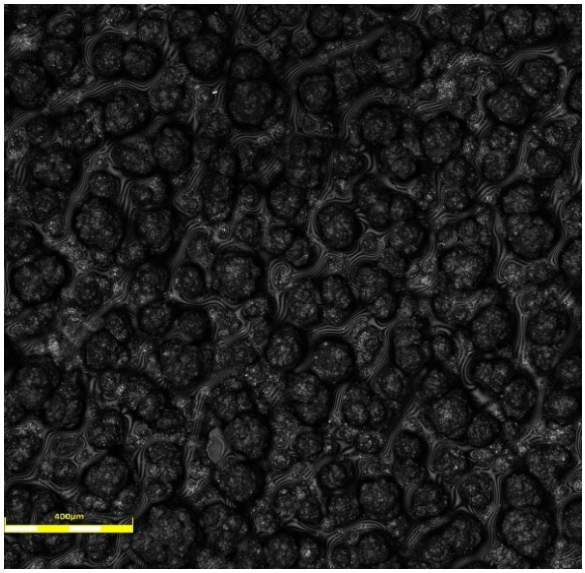

(d)

Figure 4-10 images from the confocal laser microscope, show the changes in surface composition/appearance of the samples before (Figure 4-10 a) and after oil impregnation (Figure 4-10 b) and also after the icing cycles (Fig 4-10 c) and finally after the heating process (Figure 4-10 d).

The measurement of the oil thickness has been determined by the confocal laser microscopy, the software has a feature that allows one to choose different spots on the sample's surface and measure the distance in between (e.g. create a triangle by defining three points on the surface and the software will calculate the length of the sides) Table 4-7 shows the oil's thickness results after each process. The reason behind measuring the oil's thickness is to identify the changes that happens after each step (before impregnation, after 2 hrs, after icing test, after heating) and if after the heating process we were able to increase the thickness of the oil layer it means we were able to retrieve the oil to the surface. Furthermore, heating the sample can decrease the waiting time to retrieve the oil from the micro-pillars from a matter of days to a matter of minutes (a faster self-healing feature). Finally, for the future work, having a porous coating as a first layer then develop the hierarchical structure on top of that porous layer can allows one to increase the oil reservoir capacity and having more oil kept hidden away from the harsh conditions on the surface (e.g. icing cycles).

Table 4-7 Shows the oil thickness results for each process:

Before oil impregnation (μm)	After 2 hours (μm)	After 10 cycles of icing/deicing (μm)	After heating for 10 minutes (μm)
0	150	24	40

Chapter 5. Summary and Conclusions

In this work, an experimental study was performed to investigate how a porous, oil-impregnated ceramic coating can affect the mobility of water droplets on its surface and, more specifically, how can the coating microstructure be tailored to create an efficient and durable "slippery surface" (SLIPS) after oil impregnation.

Porous TiO_2 coatings which had a hierarchal structure at the micro- and nano-scales were produced with a range of thicknesses by varying the number of plasma torch passes by suspension plasma spraying. The coatings comprised pillars of approximately 20-360 μm in height. The hierarchical structure was produced after the initial grit blasting with fine particles. The micro-pores produced between the pillars play a significant role in acting as a reservoir for the oil and allowing for some redistribution after icing. After plasma spraying, a treatment for lowering the surface energy by using stearic acid played a key role in maintaining a low CAH and SA.

Low contact angle hysteresis [CAH <10°] was achieved by using a Krytox oil with a viscosity of 250 cSt for the surface impregnation. The icing/deicing tests of the infused samples were studied and the results showed that samples infused with 250 cSt oil maintained a CAH of less than 10° for at least 5 icing/deicing cycles. It was also shown that these samples demonstrate a "self-healing" capability that can occur over time (1 week at room temperature) or be accelerated by the use of elevated temperatures (100°C) for shorter times (10 minutes). The reason behind the recovery of the slippery surface is due to rewetting the surface with oil from the micro-pockets due to the action of capillary forces.

For future work, different types of material can be used as the substrate instead of stainless steel. Improving the cooling system of the substrate holder in order to maintain the substrate's temperature will be required in this regard as uncontrolled substrate temperature can lead to coating delamination.

Furthermore, creating a larger oil reservoir beneath the coating surface can lead to preserving the oil for a longer period of time after the icing de-icing cycles. This can be applied

by having a very porous coating as a first coating layer then creating on top of it the two-level hierarchical structure.

Optimizing the oil characteristics for de-icing application is a key role to having good wettability of oil on the ceramic coating and by adding the stearic acid to lower the surface energy we can maximize the self-recovery behavior.

Finally, producing a regular substrate surface micro-morphology with laser patterning is a very promising technique and can be used as an alternative to grit blasting. This may help with producing more uniform and controllable micro-pillars. Finally, performing icing tests at higher wind speeds in the icing wind tunnel would be more representative of real aircraft icing conditions.

References

[1] Transportation Safety Board of Canada, Aviation Investigation Report A14W0181 - Severe Icing Encounter and Forced Landing, Gatineau, (2016).

[2] S.D. Green, A Study of U.S. Inflight Icing Accidents and Incidents, 1978 to 2002, 44th AIAA Aerosp. Sci. Meet, (2006).

[3] J.T, J.R. A. Heinrich, R. Ross, G. Zumwalt, J. Provorse and V. Padmanabhan, Aircraft Icing Handbook - Volume 2 of 3, National Technical Information Service, Springfield, (1991).

[4] P. Appiah-Kubi, U.S. inflight icing accidents and incidents, 2006 to 2010, Thesis, (2013).

[5] W.G.S. and P.E. D. L. Kohlmann, Icing-Tunnel Tests of a Glycol-Exuding, Porous Leading-Edge Ice Protection System. J. Aircraft, Vol. 19, No. 8, Pp. 647-654, (1982).

[6] K. Al-Khalil, Thermo-Mechanical Expulsion Deicing System-TMEDS, 45th AIAA Aerospace Sciences Meeting and Exhibit, Reno, (2007).

[7] FAA, Ice and rain protection, chapter 15, Handbook and manuals, http://www.sweethaven02.com/Aviation/MaintHandbook/ama_Ch15.pdf. (2018).

[8] N. Sharifi, M. Pugh, C. Moreau and A. Dolatabadi, Developing hydrophobic and superhydrophobic TiO2 coatings by plasma spraying, Surf. Coatings Technol, (2016).

[9] J.D. Smith, R. Dhiman, S. Anand, E. Reza-Garduno, R.E. Cohen, G.H. McKinley, K.K. Varanasi, Droplet mobility on lubricant-impregnated surfaces, Soft Matter, (2013).

[10] Paxton Juuti, Janne Haapanen, Achieving a slippery, liquid-infused porous surface with anti-icing properties by direct deposition of flame synthesized aerosol nanoparticles on a thermally fragile substrate, Appl. Phys. Lett. 110, (2017).

[11] D. Daniel, M.N. Mankin, R.A. Belisle, T.S. Wong, J. Aizenberg, Lubricant-infused micro/nano-structured surfaces with tunable dynamic omniphobicity at high temperatures, Appl. Phys. Lett. 102 (2013).

[12] P. Kim, T.S. Wong, J. Alvarenga, M.J. Kreder, W.E. Adorno-Martinez, J. Aizenberg, Liquid-infused nanostructured surfaces with extreme anti-ice and anti-frost performance, ACS Nano, (2012).

[13] T. Young, An Essay on the Cohesion of Fluids, Philos. Trans. R. Soc. London, (1805).

[14] Y.. L. T.R. Yuan, Contact Angle and Wetting Properties, Springer Ser. Surf. Sci, (2013).

[15] R. Tadmor, Line energy and the relation between advancing, receding, and Young contact

angles, (2004).

[16] N. Sharifi, F. Ben Ettouil, C. Moreau, A. Dolatabadi, M. Pugh, Engineering surface texture and hierarchical morphology of suspension plasma sprayed TiO2coatings to control wetting behavior and superhydrophobic properties, Surf. Coatings Technol. p:139–148, (2017).

[17] R.N. Wenzel, resistance of solid surfaces to wetting by water, ind. eng. chem. 28 (1936).

[18] A.B.D. Cassie, S. Baxter, Wettability of porous surfaces, Trans. Faraday Soc. 40 (1944).

[19] N. Sharifi, Developing Superhydrophobic Coatings for Anti-Icing Applications in Aerospace using Thermal Spray Processes,Thesis, (2018).

[20] L.I.E.L. Qu, Superhydrophobic states, (2003).

[21] J. Comtet, A. Niguès, V. Kaiser, B. Coasne, L. Bocquet, A. Siria, Nanoscale capillary freezing of ionic liquids confined between metallic interfaces and the role of electronic screening, 16 (2017).

[22] M. Hsu, N. Bhate, K.K. Varanasi, T. Deng, J.D. Smith, M. Hsu, N. Bhate, Frost formation and ice adhesion on superhydrophobic surfaces Frost formation and ice adhesion on superhydrophobic surfaces, 234102 (2013).

[23] P. Irajizad, M. Hasnain, N. Farokhnia, S.M. Sajadi, H. Ghasemi, Magnetic slippery extreme icephobic surfaces, Nat. Commun, 7 (2016).

[24] J.H. Kim, J.P. Rothstein, Droplet Impact Dynamics on Lubricant-Infused Superhydrophobic Surfaces: The Role of Viscosity Ratio, Langmuir, 32 (2016).

[25] G.H. Zhu, S.H. Cho, H. Zhang, M. Zhao, N.S. Zacharia, Slippery Liquid-Infused Porous Surfaces (SLIPS) Using Layer-by-Layer Polyelectrolyte Assembly in Organic Solvent, Langmuir, 34 (2018).

[26] W. Ma, Y. Higaki, H. Otsuka, A. Takahara, Perfluoropolyether-infused nano-texture: A versatile approach to omniphobic coatings with low hysteresis and high transparency, Chem. Commun, 49 (2013).

[27] J. Wang, K. Kato, A.P. Blois, T.S. Wong, Bioinspired Omniphobic Coatings with a Thermal Self-Repair Function on Industrial Materials, ACS Appl. Mater. Interfaces, 8 (2016).

[28] F.Ettouil, Modélisation rapide du traitement de poudres en projection par plasma d'arc, Thesis, (2008).

[29] D. Waldbilling och O. Kesler, Effect of suspension plasma spraying process parameters YSZ coating microstructure and permeability, Surface & Coatings Technology, Surf. Coat.

Technol, (2011).

[30] H.S. Hadi A, Y. Ando, Development of a Fabrication Process Using Suspension Plasma Spray for Titanium Oxide Photovoltaic Device, Coatings, 7 (2017).

[31] S. Metco, An Introduction to Thermal Spray, (2013).

[32] A. Ganvir, Microstructure and Thermal Conductivity of Liquid Feedstock Plasma Sprayed Thermal Barrier Coatings, (2016).

[33] Pierre L. Fauchais, Thermal Spray Fundamentals, (2014).

[35] A.F. Stalder, G. Kulik, D. Sage, L. Barbieri, P. Hoffmann, A snake-based approach to accurate determination of both contact points and contact angles, Colloids Surfaces A Physicochem. Eng. Asp, 286 (2006).

[36] A.F. Stalder, T. Melchior, M. Müller, D. Sage, T. Blu, M. Unser, Low-bond axisymmetric drop shape analysis for surface tension and contact angle measurements of sessile drops, Colloids Surfaces A Physicochem. Eng. Asp, 364 (2010).

[37] 3MB Plasma Spray Gun, Oerlikon, Metco (2016). http://oerlikon.com/metco/en/products-services/coating-equipment/thermal-spray/spray-guns/coating-equipment-plasma/3mb/